NMR Studies on Two-Dimensional Molecular Conductors and Superconductors: Mott Transition in κ-(BEDT-TTF)$_2$X

Kazuya Miyagawa and Kazushi Kanoda*

Department of Applied Physics, University of Tokyo, Hongo 7-3-1, Bunkyo-ku, Tokyo 113-8656, Japan, and CREST-JST

Atsushi Kawamoto

Department of Physics, Hokkaido University, Kita-ku, Sapporo, Hokkaido 060-0810, Japan

Received July 19, 2004

Contents

1. Introduction: κ-(BEDT-TTF)$_2$X Situated around the Mott Transition

Most familiar molecular conductors are composed of a conducting subsystem of donor molecules (D) and a nonconducting subsystem of monovalent anion molecules (A) with a form of D_2A, where the carrier concentration is half a hole per donor molecule. Even if the carrier density is fixed, the molecular conductors exhibit a variety of ground states such as spin density wave, charge density wave, spin−Peierls, magnetically ordered, metallic, and superconducting states. The source of the variation is the mutual interplay between the low dimensionality, the electron correlations, the electron−phonon interaction, the electron kinetic energy (transfer integral), and the topology of the Fermi surface. The relative importance of the ingredients is controlled by the molecular arrangement in the real material. When the donor molecules are strongly dimerized in the conducting subsystem, the band filling gets effectively half-filled and the competition between the electron−electron Coulomb repulsion and the kinetic energy is highlighted, resulting in the Mott transition between insulating or metallic states. This phase competition has been extensively studied because the correlation-driven metal−insulator transition is one of the central issues in condensed matter physics. Moreover, it has come to a common recognition that superconductivity is enhanced around the Mott transition. Thus, the Mott transition is not only an issue of basic physics but also a phenomenon which attracts chemists engaged in novel material synthesis.

Organic conductors are model systems suitable for research of the electron correlations because the van der Waals nature of the molecular packing allows precise control of the transfer integral relative to the Coulomb repulsive energy by chemical substitution or physical pressure. In this article, we review NMR studies on quasi-two-dimensional organic conductors in light of the physics of the Mott transition.

The compounds which we are focusing on in this article are a family of κ-(BEDT-TTF)$_2$Xs, which is abbreviated to κ-X. They are layered materials composed of conducting layers with $^1/_2$ hole per BEDT-TTF and insulating layers of various monovalent anions, X^-, as shown in Figure 1a. The anion, X^-, forms a closed shell, which has no contribution to electronic conduction nor magnetism. In the conducting layer, BEDT-TTF molecules form a dimer, which is arranged in a checkerboard pattern (Figure 1b). Since a dimer carries a hole, the electronic band constructed by the dimers is half-filled. This view of the electronic structure is supported by band structure calculations; namely, two BEDT-TTF HOMOs in the dimer are split into bonding and antibonding orbitals, each of which forms a conduction band due to the interdimer transfer integrals. As was given in the band structure calculations,[1] the two bands are separated by a finite gap so that the relevant band for hole filling is only the antibonding band, which is half-filled by one hole per dimer. The two-particle (hole) energy level in a dimer Hubbard model is given by

$$E_2 = 2\epsilon_0 + \frac{U_{\mathrm{ET}}}{2}\left[1 - \sqrt{1 + \left(\frac{4t_{\mathrm{dimer}}}{U_{\mathrm{ET}}}\right)^2}\right]$$

where ϵ_0 is the HOMO level, U_{ET} is the on-site Coulomb energy of the BEDT-TTF molecule, and t_{dimer} is the intradimer transfer energy. Because the one-particle (hole) ground-state level is $E_1 = \epsilon_0 - t_{\mathrm{dimer}}$, the on-dimer Coulomb energy U_{eff} is $E_2 - 2E_1$,

* Corresponding author. University of Tokyo. Phone: 81-3-5841-6830. Fax: 81-3-5841-8808. E-mail: kanoda@ap.t.u-tokyo.ac.jp.

10.1021/cr0306541 CCC: $48.50
Published on Web 10/27/2004

K. Miyagawa is a Research Associate of Applied Physics at the University of Tokyo in Japan. He received his Ph.D. from the University of Tokyo in 2003.

K. Kanoda is a Professor of Applied Physics at the University of Tokyo in Japan. He received his Ph.D. from Kyoto University in 1987.

A. Kawamoto is an Associate Professor of Physics at Hokkaido University in Japan. He received his Ph.D. from Nagoya University in 1992.

which yields $2t_{dimer}$ in the limit of $U_{ET} \gg t_{dimer}$.[2] In κ-X, $U_{ET} \sim 1$ eV and $t_{dimer} \sim 0.25$ eV.[3] Applying this formula to κ-X, U_{eff} is estimated at 0.5 eV. On the other hand, the bandwidth, W, is determined by the interdimer transfer integral, t', and roughly given by $2z(t'/2)$, where z is the number of nearest-neighbor dimers and $t'/2$ is the transfer integral between the neighboring antibonding orbitals. For κ-(BEDT-TTF)$_2$X, $t' \sim 0.1$ eV and $z = 6$ yield $W \sim 0.6$ eV. So, U_{eff}/W is of the order of unity. Although this is an order of estimate neglecting other effects such as intersite Coulomb repulsion V and screening effects, this suggests that κ-X is likely in the critical region of the Mott transition.[4]

It is well-known that the bandwidth of κ-X is varied by replacement of X. The occurrence of a Mott transition is demonstrated in the resistivity behaviors of the three representative salts of κ-Cu(NCS)$_2$, κ-Cu[N(CN)$_2$]Br, and κ-Cu[N(CN)$_2$]Cl, as shown schematically in Figure 2a. The κ-Cu(NCS)$_2$ and κ-Cu[N(CN)$_2$]Br are metals with superconducting transitions at low temperatures, while κ-Cu[N(CN)$_2$]Cl is a Mott insulator. Moreover, progressive deuteration of κ-Cu[N(CN)$_2$]Br causes the system to approach the Mott border, and the fully deuterated κ-Cu[N(CN)$_2$]-Br reaches just the border of the Mott transition, as found by Taniguchi et al. (see Figure 2b).[5] The above considerations and the resistive behaviors lead to a conceptual phase diagram for BEDT-TTF compounds with strongly dimeric molecular arrangements, as

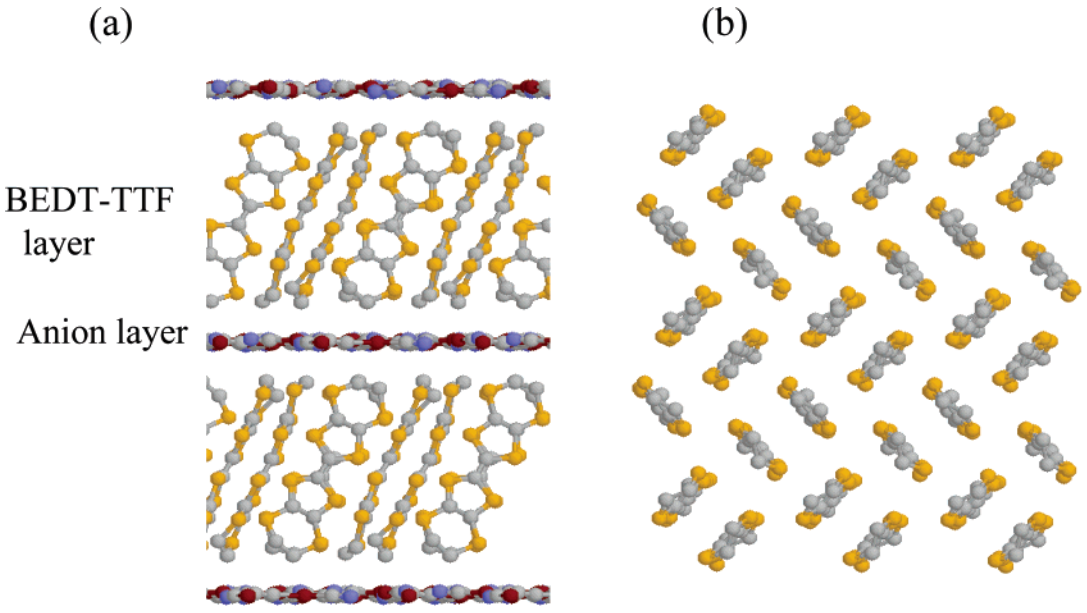

Figure 1. (a) Layered crystal structure of κ-(BEDT-TTF)$_2$X. (b) BEDT-TTF arrangement in the conducting layer.

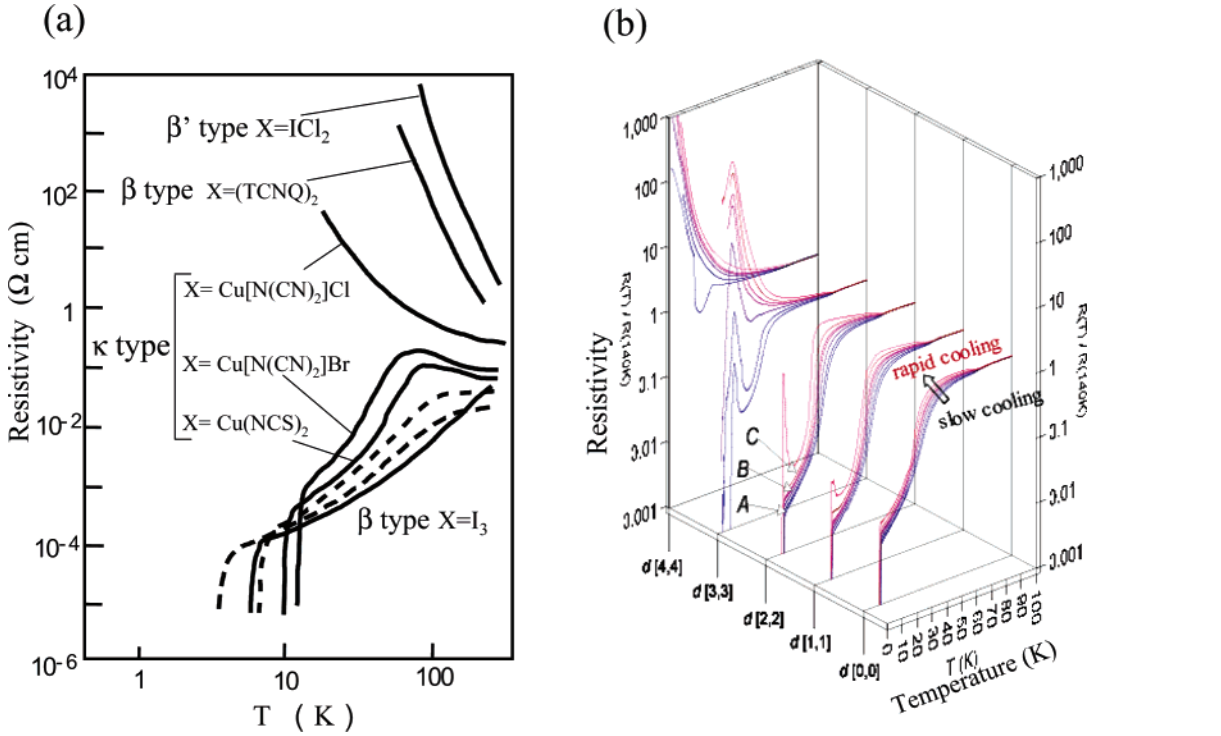

Figure 2. (a) Resistivity behaviors of dimeric (BEDT-TTF)$_2$X including κ-(BEDT-TTF)$_2$X. (b) Resistivity behaviors of κ-(BEDT-TTF)$_2$Cu[N(CN)$_2$]Br with different degrees of deuteration denoted by d[*n*.*n*], which means that *n* protons out of four in each ethylene group located on both sides of BEDT-TTF are deuterated. The cooling-rate dependence of the resistive behavior is related to change and/or disorder in transfer integrals caused by the ethylene group conformational disorder, whic depends on the freezing speed. (Part b is reprinted with permission from ref 5. Copyright 1999 American Physical Society.)

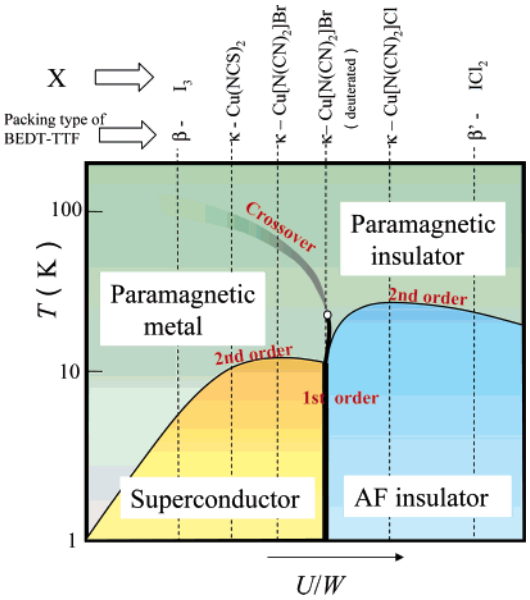

Figure 3. Conceptual phase diagram for (BEDT-TTF)$_2$X with dimeric donor structures. The materials to be dealt with here can be situated as shown.

depicted in Figure 3.[2,6] The κ-Cu(NCS)$_2$, κ-Cu[N(CN)$_2$]-Br, and κ-Cu[N(CN)$_2$]Cl are across the Mott border.[7] Therefore, close investigation of the four members is expected to provide a deep understanding of the Mott physics. The concern of the present article is how to tackle this issue with NMR experiments.

This paper is organized as follows: In section 2, several fundamentals of NMR on BEDT-TTF compounds are given. In section 3, the overall behaviors of the four members are revealed by NMR study on powdered specimens. The ground state in the metallic phase, namely the superconducting state, is discussed in section 4. The detailed characterization of the ground state in the insulating phase, which is antiferromanet, is described in section 5. The electronic state on the Mott border is revealed by the study of the deuterated κ- Cu[N(CN)$_2$]Br in section 6. Section 7 concludes this paper with some words on perspectives.

2. NMR Fundamentals of BEDT-TTF Compounds

The BEDT-TTF molecule, with the chemical formula $C_{10}S_8H_8$, is shown in Figure 4a. Since the naturally abundant isotopes, ^{12}C and ^{32}S, have no nuclear spins, most of NMR studies on the BEDT-TTF based compounds had been performed at ^1H sites (nuclear spin $^1/_2$). However, the ^1H sites have such a small hyperfine coupling with conduction

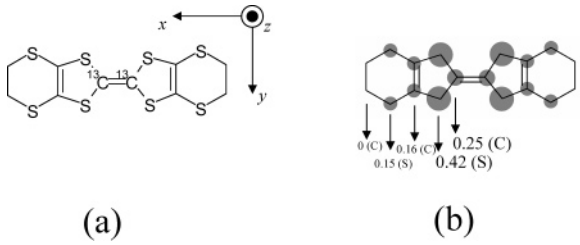

Figure 4. (a) Structure of the BEDT-TTF molecule. The axes shown are principal ones defined for the NMR hyperfine coupling tensor described later. (b) Calculated population densities of the HOMO.[8] The sizes of circles represent the populations.

Table 1. Characteristics of Nuclei Available for NMR in the BEDT-TTF Molecule

nucleus	I	$\gamma/2\pi$ (MHz/T)	HOMO density	abundance(%)
^{1}H	$^{1}/_{2}$	42.5774	very small	99.985
^{13}C (center)	$^{1}/_{2}$	10.7054	large	1.11
^{33}S (center)	$^{3}/_{2}$	3.2655	largest	0.75

carriers that the Knight shift cannot be resolved in the paramagnetic state. Moreover, the dynamics of the ethylene groups containing ^{1}H overwhelms the electronic contribution to the relaxation rate at high temperatures. So, the ^{1}H sites of BEDT-TTF compounds are not suitable for getting information on the electronic states, while they can be a good probe of the molecular motion and the vortex dynamics. NMR study at sites with much higher carrier density is desirable. The calculated spin-density distribution of the HOMO in BEDT-TTF is shown in Figure 4b.[8] It is seen that the density is high in the central area of BEDT-TTF. We summarize in Table 1 the nuclear spin, the magnetogyric ratio, γ, the population density of the HOMO, and the natural abundance of NMR-available nuclei in BEDT-TTF molecules.

It is well-known that when the nuclear spin is larger than $^{1}/_{2}$, the quadrupole moment, Q, affects the shape of spectra and the relaxation rate.[9] It is often difficult to discuss the electronic properties in terms of the observed NMR data due to this quadrupole effect. Moreover, the small γ value of ^{33}S makes it difficult to observe its NMR signals. So, we chose the central carbon sites for NMR study and enriched ^{13}C isotopes at the central carbon sites in the BEDT-TTF molecule, as shown in Figure 4a.

The hyperfine field at the central carbon site consists of the isotropic Fermi contact field due to the core polarization, the on-site $2p_z$ dipole field, and the off-site dipole field from one adjacent carbon and two adjacent sulfur sites. So, the hyperfine field tensor A defined for a one-electron spin on the BEDT-TTF molecule is expressed as

$$A = \sigma_c \begin{pmatrix} \alpha - \beta_{2p_z} & 0 & 0 \\ 0 & \alpha - \beta_{2p_z} & 0 \\ 0 & 0 & \alpha + 2\beta_{2p_z} \end{pmatrix} + \sigma_c \begin{pmatrix} 2\beta_c & 0 & 0 \\ 0 & -\beta_c & 0 \\ 0 & 0 & -\beta_c \end{pmatrix} + 2\sigma_s \begin{pmatrix} (1+3\cos\delta)\beta_s/2 & 0 & 0 \\ 0 & (1+3\cos\delta)\beta_s/2 & 0 \\ 0 & 0 & -\beta_s \end{pmatrix} \quad (1)$$

where the x-, y-, and z-axes are taken as shown in Figure 4a and are the principal axes of the hyperfine field tensor. The first term is the on-site contribution, where α is an isotropic core-polarization field and β_{2p_z} is an on-site dipole field given by $2\langle\mu_B/r^3\rangle/5$, which is known to be 43 kOe. The second and third ones are the off-site dipole contributions from neighboring carbon and sulfur atoms, respectively. In the point dipole approximation, the off-site dipole field, $\beta_C = \mu_B/r_{C=C}^3$ and $\beta_S = \mu_B/r_{C-S}^3$, is estimated at 3.8 and 1.8 kOe using the bond lengths in the BEDT-TTF molecule.[10] δ is the bond angle of S$-^{13}$C$-$S. σ_C and σ_S are the spin densities on the carbon and sulfur atoms for one spin on the BEDT-TTF HOMO. According to molecular orbital calculations, the Mulliken populations at the carbon and sulfur sites in question are 0.06 and 0.17.[11] If we use these values to estimate the anisotropic terms, the principal values of the tensor yield $A = (a - 2.1, a - 2.1, a + 4.2)$ in units of kOe. The isotropic term a is estimated at 1.3 kOe/μ_B from the observed central shift of 60 ppm and the spin susceptibility per BEDT-TTF molecule, χ_{spin}, of 2.5×10^{-4} emu/mol at room temperature. Then, A yields $(-0.7, -0.7, 5.5)$.

Experimentally, the hyperfine field tensor is determined from the Knight shift tensor, which was measured by Mayaffre et al.[12] and Soto et al.[13] through detailed examination of the field-angular dependence of NMR spectra for the κ-Cu[N(CN)$_2$]Br crystal. In an isolated BEDT-TTF molecule, the two central carbon sites are equivalent. In the κ-Cu[N(CN)$_2$]Br crystal, however, they are inequivalent because two BEDT-TTF molecules form an inclined dimer in the conducting layer. Actually, the observed angular dependence of the spectra was attributed to the two ^{13}C sites with different shift tensors. Referring to the susceptibility (2.5×10^{-4} emu/mol), the obtained shift tensors are reduced to the hyperfine field tensors (in units of kOe) for one spin on BEDT-TTF as follows: $(-4,4, -2.7, 7.9)$ and $(-0.5, 0.5, 14)$ in ref 12; $(-1.4, -3.3, 10)$ and $(1.4, 0.8, 18)$ in ref 13. Although there is a quantitative difference between the two groups, it is commonly seen that the hyperfine field has a large anisotropy. One finds a large discrepancy between the experimental and calculated values. It is partially because the real spin densities at the central carbon and sulfur sites are in reality much larger that the MO calculations, because the point charge approximation in the calculation of the dipole field is inappropriate, or because the spin on the counter molecule in the dimer affects the hyperfine field. In connection to the last possibility, the principal axes of the field tensor are suggested to be rotated from the molecular axes.[12,13]

The ^{13}C-enriched BEDT-TTF molecule shown in Figure 4a was synthesized from $^{13}CS_2$ according to the method by Larsen and Lenoir[14] with some modification. For ^{13}C NMR studies of the fully deuterated κ-Cu[N(CN)$_2$]Br, the hydrogens in the ethylene group are substituted by deuterium as well as the ^{13}C enrichment. The BEDT-TTF molecules were recrystallized from chlorobenzene. Examination of the mass spectrum of the product confirmed the successful substitution.

3. Overall Behaviors of κ-(BEDT-TTF)$_2$X

As seen above, the ^{13}C nucleus in BEDT-TTF has an anisotropic hyperfine coupling tensor. As the BEDT-TTF geometry against the crystal axes depends on X, one cannot attain the same field-molecule geometry even if the field is aligned to the same crystal axis for different compounds. For quantitative comparison of the NMR shift and relaxation data of

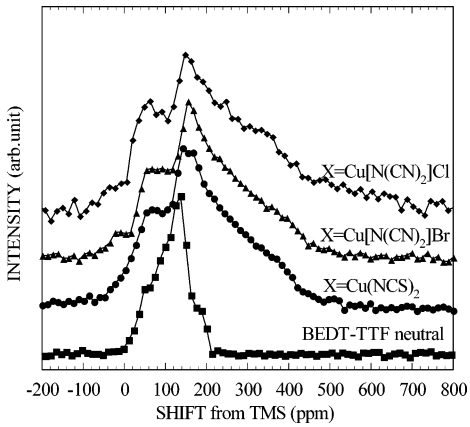

Figure 5. ^{13}C NMR spectra for powdered samples of three κ-phase BEDT-TTF salts and neutral BEDT-TTF molecules at room temperature. (Reprinted with permission from ref 15. Copyright 1995 American Physical Society.)

the four members, the magnetic field has to be aligned to the same geometry relative to the BEDT-TTF molecule for all members to maintain the same hyperfine tensor against the magnetic field. Since the molecular configurations with respect to the crystal axes are different for these salts, to ensure this condition for the members is not so straightforward. Alternatively, the experiments on powdered samples are effective because the angular effect of the hyperfine tensor is averaged. To compare the overall behaviors of the four members, we performed powder experiments.

The ^{13}C NMR spectra for powdered κ-Cu(NCN)$_2$, κ-Cu[N(CN)$_2$]Br, and κ-Cu[N(CN)$_2$]Cl and neutral BEDT-TTF at room temperature are shown in Figure 5 .[15] The observed spectra for the κ-phase salts have nearly the same central shift and uniaxial symmetry except for the apparent splitting of the peak around 100 ppm. These similarities of spectra indicate that the electronic characters are nearly the same, at least at room temperature. The uniaxial symmetry is consistent with the nearly equal values of the x- and y-axes principal values of the total shift tensor, which sums the chemical and Knight shift tensors. The peak splitting is reasonably understood by the difference of the shift values between the two inequivalent carbon sites.

As seen in Figure 5, the anisotropy (measured by the spectral width) of the observed shift in κ-(BEDT-TTF)$_2$X is much greater than the anisotropy of the chemical shift, and therefore, the temperature and X dependence of the Knight shift is reflected in the width of the spectra. Figure 6 shows the peak-to-peak width of the dispersion curve as a function of temperature.[15] The magnitude and the temperature dependence are common to all three salts except for the low-temperature region of κ-Cu[N(CN)$_2$]Cl, which shows anomalous broadening due to magnetic ordering (see below). These behaviors are compared to the spin susceptibilities of polycrystals of three salts shown in Figure 7, where the diamagnetic core contribution of $\sim 4.7 \times 10^{-4}$ emu/mol of dimer for the three compounds is corrected. The magnitude and temperature dependence are similar for the three salts, except for the κ-Cu[N(CN)$_2$]Cl salt below 30 K,

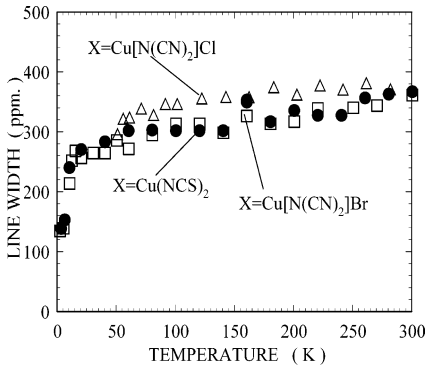

Figure 6. Temperature dependence of the line width of ^{13}C NMR spectra in three κ-phase compounds. (Reprinted with permission from ref 15. Copyright 1995 American Physical Society.)

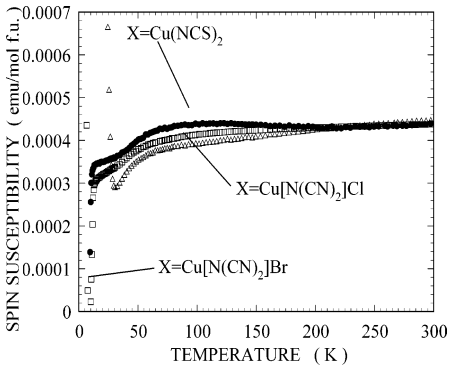

Figure 7. Temperature dependence of static susceptibility of κ-phase salts per formula unit. (Reprinted with permission from ref 15. Copyright 1995 American Physical Society.)

where a weak ferromagnetic phase transition occurs. The susceptibility remains constant above $\sim$100 K and decreases gradually at low temperatures. These behaviors are in agreement with the previous reports on the κ-Cu(NCS)$_2$ salt[16] and the κ-Cu[N(CN)$_2$]Cl salt.[17] Comparing Figures 6 and 7, the NMR spectral width for the three salts is seen to be scaled to the spin susceptibility except for the κ-Cu[N(CN)$_2$]Cl salt at low temperatures. The accurate measurements of the temperature dependence of the Knight shift using a single crystal were performed for κ-Cu[N(CN)$_2$]Br by Mayaffre et al.[12] and De Soto et al.,[13] who reproduced the whole temperature dependence and clearly identified the anolamous decrease of the Kight shift at low temperatures, consistent with the susceptibility behavior.

The temperature dependence of the line shape for powdered κ-Cu[N(CN)$_2$]Cl is shown in Figure 8.[15] Above 60 K, the line shape is similar to those of the other κ-phase compounds. However, as the magnetic order is approached, the spectra broaden despite the gradual decrease in the spin susceptibility as seen in Figure 7, indicating an antiferromagnetic nature of the magnetic ordering. When the magnetic phase transition occurs at 27 K, the spectra spread out of the experimental frequency. We cannot enter into details of the ordered state with the powder data described in this section. The characterization of the ordered state was probed by the single-crystal NMR experiment, which will be presented in sections 5 and 6.

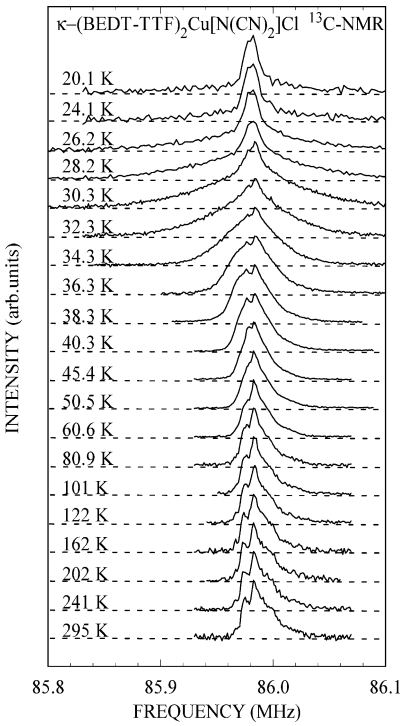

Figure 8. Temperature dependence of ^{13}C NMR spectra of κ-Cu[N(CN)$_2$]Cl. (Reprinted with permission from ref 15. Copyright 1995 American Physical Society.)

Next, we discuss the NMR relaxation rate, $1/T_1$, in the powder experiments.[15] First, let us consider a simple case of hyperfine field tensor of uniaxial symmetry with principal values of $(a - B, a - B, a + 2B)$, where a and B are isotropic and anisotropic terms. The local field fluctuations perpendicular to the external field are expressed by

$$\langle \delta H(\tau)\, \delta H(0)\rangle_\theta = \sum_q \{[4a_q a_{-q} - (1 + 3\cos 2\theta)(a_q B_{-q} + a_{-q} B_q) + (7 - 3\cos 2\theta) B_q B_{-q}]/4\} \langle \sigma_q(\tau)\, \sigma(0)\rangle \quad (2)$$

where a_q and B_q are matrix elements of a and B with a scattering vector of q, $\langle \sigma_q(\tau)\, \sigma_{-q}(0)\rangle$ is the correlation function of the spin density on BEDT-TTF, and θ is the angle between the external field and the symmetry axis.[15] As seen in this formula, the fluctuations depend on θ due to the strong anisotropy of the hyperfine tensors, and therefore, the relaxation rate of the nuclear magnetization should depend on θ. By performing the experiments on powder, one can eliminate the angular effect, which is not of significance for the present study. However, the observed recovery curve of the nuclear magnetization for the powdered sample does not obey the single-exponential function of time. Then, we define the nuclear-spin relaxation time, T_1^0, from the initial slope of the relaxation curve. It is calculated analytically, based on eq 3.3, and yields

$$(T_1{}^0)^{-1} \equiv \left(\frac{\partial \ln M_z(t)/M_\infty}{\partial t}\right)_{t=0} = \frac{\gamma_I{}^2}{2}\sum_q (a_q a_{-q} + 2B_q B_{-q}) \int \mathrm{d}\tau\, \langle \sigma_q(\tau)\, \sigma_{-q}(0)\rangle \cos \omega\tau \quad (3)$$

where $M_z(t)$ is the nuclear magnetization. Expressing the correlation function in terms of the dynamic susceptibility, a relationship between $T_1{}^0$ and the dynamic susceptibility is given as

$$\frac{1}{T_1{}^0 T} = \frac{k_B \gamma_I{}^2}{\gamma_e{}^2 \hbar^2} \sum_q (2a_q a_{-q} + 4B_q B_{-q}) \frac{\chi''_q(\omega)}{\omega} \quad (4)$$

The above procedure can be followed even in the general case of the hyperfine field with the three principal values all different, as denoted by $(a - B1, a - B2, a + B1 + B2)$. The resultant form is

$$\frac{1}{T_1{}^0} = \frac{k_B \gamma_I{}^2 T}{2\gamma_e{}^2 \hbar^2} \sum_{i,q} \{[2{}^iA_q{}^iA_q + 2(2{}^iB1_q{}^iB1_{-q} + {}^iB1_q{}^iB2_{-q} + {}^iB2_q{}^iB2_{-q} + 2{}^iB2_q{}^iB2_{-q})]/3\} \frac{\chi''(q,\omega)}{\omega} \quad (5)$$

where i (=1,2) denotes either of the two carbon sites in the BEDT-TTF molecule. The form is somewhat complicated. However, the useful consequence of the equation is that the relaxation rate determined by the powder NMR experiments is proportional to the dynamic spin susceptibility and is used for quantitative comparison of different salts, assuming that the hyperfine field tensor is the same for κ-X. When only the uniform part is considered in the summation, the equation turns out to be a Korringa's relation extended to the case of the anisotropic hyperfine coupling as follows:

$$\frac{T_1{}^0 T}{2} \sum_i \{{}^iK_{iso}{}^2 + [2({}^iK_{aniso,11}{}^2 + {}^iK_{aniso,11}{}^iK_{aniso,22} + {}^iK_{aniso,22}{}^2)]/3\} = \left(\frac{\gamma_e}{\gamma_I}\right)^2 \left(\frac{\hbar}{4\pi k_B}\right) \quad (6)$$

where K_a, K_{B1}, and K_{B2} are the corresponding Knight shifts. Referring to the observed shift tensors,[12] the Korringa relation yields the value $1/(T_1{}^0T) = 0.017$ s^{-1} K^{-1}, which is expected in the absence of electron correlation.

Let's turn our attention to the experimental results. The temperature dependence of $1/(T_1{}^0T)$ for the three compounds is shown in Figure 9.[15] The most prominent feature is a divergent peak at 27 K for κ-Cu[N(CN)$_2$]Cl. This indicates a magnetic ordering. The temperature dependence above 27 K in κ-Cu[N(CN)$_2$]Cl salt is considered to originate from critical magnetic fluctuations. This behavior is common to the three salts above 60 K, meaning that the magnetic spin fluctuations survive even in the 10 K-class superconductors of κ-Cu(NCS)$_2$ and κ-Cu[N(CN)$_2$]Br at high temperatures. The turnabout of $1/(T_1{}^0T)$ below 55 K for κ-Cu(NCS)$_2$ and below 45 K for κ-Cu[N(CN)$_2$]Br is an indication of the suppression of the spin fluctuations. These temperatures coincide with the inflection point in the temperature dependence of resistivity; namely, the change of the spin fluctuations is associated with the insulator−metal crossover. The sudden decrease of $1/(T_1{}^0T)$ below ~10 K

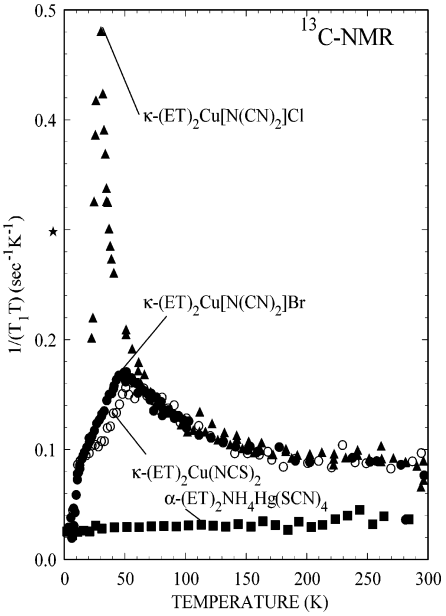

Figure 9. $1/(T_1{}^0T)$ vs temperature for three κ-phase salts and α-(BEDT-TTF)$_2$NH$_4$Hg(SCN)$_4$. For the definition of $T_1{}^0$, see the text.[6,15] (Reprinted with permission from ref 15. Copyright 1995 American Physical Society.)

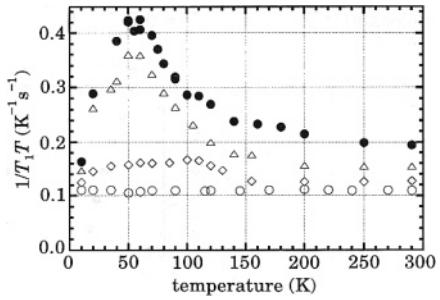

Figure 10. Pressure dependence of $1/(T_1T)$ at the ^{13}C site for κ-Cu[N(CN)$_2$]Br measured by Mayaffre et al.[12] The closed circles, open triangles, open diamonds, and open circles stand for data at pressures of 1 bar, 1.5 kbar, 3 kbar, and 4 kbar, respectively. (Reprinted with permission from ref 12. Copyright 1994 EDP Sciences.)

for κ-Cu(NCS)$_2$ and κ-Cu[N(CN)$_2$]Br is due to the superconducting transition.

The experimental values above T_C are greater than 0.09 s^{-1} K^{-1}. This is enhanced by one or half an order of magnitude over the expectation from the Korringa law. A similar enhancement factor in $1/(T_1{}^0T)$ is deduced in the single-crystal experiment for κ-Cu[N(CN)$_2$]Br.[13] It is considered that the anomalous temperature dependence and enhancement of $1/(T_1{}^0T)$ in the two superconducting salts come from aniferromagnetic spin fluctuations with finite q vectors, as observed in κ-Cu[N(CN)$_2$]Cl. It is emphasized that a large enhancement in $1/(T_1{}^0T)$ still remains just above the superconducting transition and is an indication of the highly correlated nature of the metallic phase. Indeed, the $1/(T_1{}^0T)$ of α-(BEDT-TTF)$_2$NH$_4$Hg(SCN)$_4$, which is believed to be a good metal, is several times smaller than that of the κ-phase compounds (Figure 9).

The pressure study of the single-crystal κ-Cu[N(CN)$_2$]Br performed by Mayaffre et al.[12] is informative; Figure 10 shows $1/(T_1T)$ at the ^{13}C site under

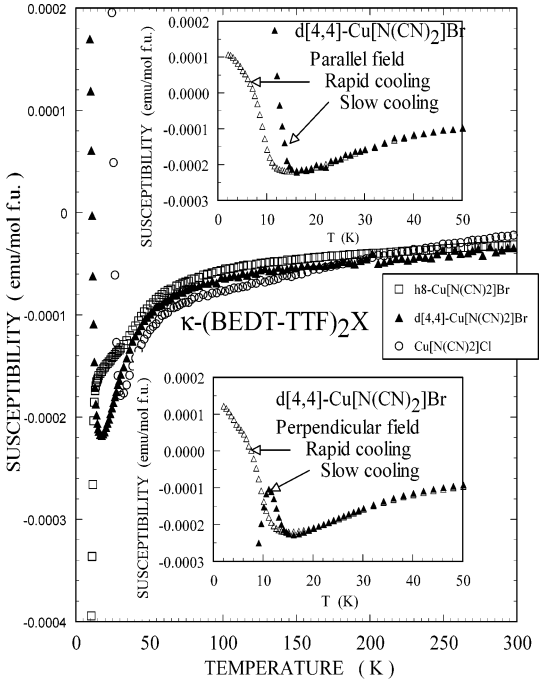

Figure 11. Temperature dependence of the dc susceptibilities of κ-Cu[N(CN)$_2$]Br, κ-d[4,4]-Cu[N(CN)$_2$]Br, and κ-Cu[N(CN)$_2$]Cl. The diamagnetic core contribution is -4×10^{-4} emu/(mol f.u.) for the three salts. The upper and lower insets show the results of κ-d[4,4]-Cu[N(CN)$_2$]Br in a field parallel and perpendicular to the layer, respectively. In both field geometries, a cooling-rate dependence appears due to a change in the superconducting volume fraction and the spin canting property in the insulating phase. (Reprinted with permission from ref 18. Copyright 1997 American Physical Society.)

several pressures. It is seen that the peak of $1/(T_1T)$ around 50 K observed at ambient pressure is depressed at higher pressures and at the same time the low-temperature value just above T_C is decreased. This observation is related to the fact that under pressures the meta-insulator crossover in resistivity becomes vague with the crossover temperature shifts toward higher temperatures. The results indicate that the system goes away from the Mott boundary and gets to behave like a usual metal under pressure.

As we explained in section 1, the fully deuterated κ-Cu[N(CN)$_2$]Br (denoted by κ-d[4,4]-Cu[N(CN)$_2$]Br) is suggested to be just on the Mott transition according to its resistivity behavior. This should be further explored. Figure 11 shows the dc susceptibility of a powdered sample.[18] At higher temperatures above 16 K, κ-d[4,4]-Cu[N(CN)$_2$]Br salt shows nearly the same behavior as κ-Cu[N(CN)$_2$]Br and κ-Cu[N(CN)$_2$]Cl; it should be said that the susceptibility of κ-d[4,4]-Cu[N(CN)$_2$]Br is between those of the other members if the data are looked at closely. Below 16 K, the susceptibility exhibits a huge increase similar to the antiferromagnetic transition with spin canting in κ-Cu[N(CN)$_2$]Cl although the transition temperature differs. The κ-d[4,4]-Cu[N(CN)$_2$]Br salt is likely to contain a considerable fraction of the electronic phase with the same magnetic character as in κ-Cu[N(CN)$_2$]-Cl. Interestingly, the low-temperature susceptibility of this boundary material is strongly affected by the cooling speed, as seen in the insets of Figure 11, which show the susceptibility after slow cooling (0.2

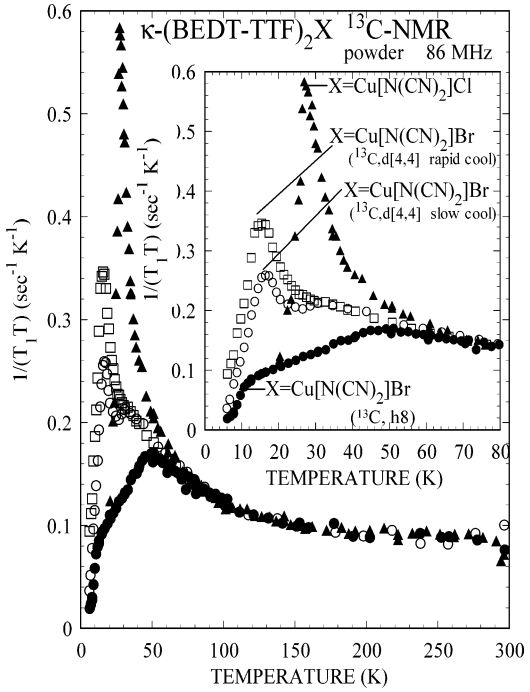

Figure 12. ^{13}C nuclear spin−lattice relaxation rate, $1/(T_1{}^0T)$, for powdered samples of κ-Cu[N(CN)$_2$]Br, κ-d[4,4]-Cu[N(CN)$_2$]Br, and κ-Cu[N(CN)$_2$]Cl. The low-temperature region is expanded in the inset. (Reprinted with permission from ref 18. Copyright 1997 American Physical Society.)

K/min) and rapid cooling (100 K/min) under fields parallel and perpendicular to the conducting layers. After the slow cooling, the susceptibility shows a minimum at 16−17 K and a steep increase due to the magnetic transition under parallel field, while the susceptibility again decreases below 11 K due to a superconducting transition under perpendicular field. The contrasting behaviors suggest that weak ferromagnetic and superconducting phases are coexistent. The absence of the diamagnetism under the parallel field is understood in terms of the large out-of-plane (Josephson-like) penetration depth (0.2 mm for κ-Cu[N(CN)$_2$]Br[19]) and realization of the vortex lock-in state. After the rapid cooling, the volume fraction of the superconducting phase is suppressed, as seen in the perpendicular-field data. At the same time, the spin canting is depressed, as seen in the parallel-field data. The fast cooling is considered to induce disorder in the ethylene conformation and concomitant change of the bandwidth. It is likely that the disorder affects the spin canting and the bandwidth changes the relative volume fractions in the material just on the Mott transition line.

The $1/(T_1{}^0T)$ of the κ-d[4,4]-Cu[N(CN)$_2$]Br powder is plotted along with the data of the superconductor, κ-Cu[N(CN)$_2$]Br, and the Mott insulator, κ-Cu[N(CN)$_2$]-Cl, in Figure 12.[18] From room temperature down to 60 K, the data of κ-d[4,4]-Cu[N(CN)$_2$]Br are on the common curve, and below 60 K, they are between those of κ-Cu[N(CN)$_2$]Br and κ-Cu[N(CN)$_2$]Cl. This indicated that κ-d[4,4]-Cu[N(CN)$_2$]Br is situated in the critical region between the metallic and Mott insulating phases. The peak formation around 15 K is attributed to the antiferromagnetic transition. All these NMR features are totally consistent with implications of the susceptibility data. The cooling

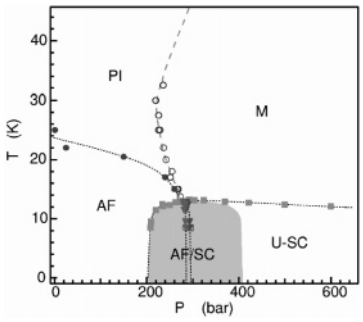

Figure 13. Temperature−pressure phase diagram of κ-Cu[N(CN)$_2$]Cl constructed by Lefebvre et al. through measurements of ^{1}H NMR and the ac shielding response. PI, AF, M, and SC stand for paramagnetic insulating, antiferromagnetic, metallic, and superconducting phases, respectively. (Reprinted with permission from ref 20. Copyright 2000 American Physical Society.)

rate dependence of $1/(T_1{}^0T)$ is interpreted by the change of the metallic and insulating phase fractions because the determined relaxation rate is some average of the values of each phase.

For investigation of the close vicinity of the Mott transition, application of pressure is also useful. Lefevbre et al. performed single-crystal ^{1}H NMR experiments on κ-Cu[N(CN)$_2$]Cl under pressure.[20] They pursued the NMR spectra and relaxation behavior as well as the ac shielding response under pressure and then constructed the pressure−temperature phase diagram shown in Figure 13.[20] By pressure, the insulating phase undergoes the Mott transition to the metallic phase, and the magnetic phase at low temperatures is converted into the superconducting phase, as in Figure 3. The pressure study and the chemical substitution are complementary to each other. The κ-d[4,4]-Cu[N(CN)$_2$]Br at ambient pressure can be regarded to sit on the boundary in Figure 13.

As seen above, the powder NMR study revealed that κ-Cu(NCS)$_2$ and κ-Cu[N(CN)$_2$]Br are strongly correlated metals, κ-Cu[N(CN)$_2$]Cl is an antiferromagnetic insulator, and κ-d[4,4]-Cu[N(CN)$_2$]Br is situated between the two phases. In the subsequent sections, exploration of each phase through a single-crystal experiments is described.

4. Superconducting State

Superconductivity emerges in the strongly correlated metallic phase of κ-X in the vicinity of the Mott transition. The pairing symmetry of the Cooper pair, which is closely related to the mechanism of the superconductivity, is of keen interest. There are various experiments to probe the symmetry of the superconducting pairing: the temperature and field dependence of the penetration depth, the electronic specific heat and the thermal conductivity, and the angular dependence of scanning tunneling spectroscopy (STS) and millimeter-wave absorption. Much experimental research on κ-X (X = Cu(NCS)$_2$ and X = Cu[N(CN)$_2$]Br) has so far been reported. However, their results are controversial; some suggest conventional s wave pairing, while some others support unconventional pairing, as is tabulated in Table 2. NMR is another probe to characterize the nature of

Table 2. Present Status of Research on the Pairing Symmetry in κ-X

	Penetration Depth		
ac susceptibility	Kanoda et al.[21]	non-s	Cu[N(CN)$_2$]Br
	Carrington et al.[22]	non-s	Cu[N(CN)$_2$]Br, Cu(NCS)$_2$
	Pinteric et al.[23]	non-s	Cu[N(CN)$_2$]Br
	Pinteric et al.[24]	non-s	Cu[N(CN)$_2$]Br
μSR	Harshman et al.[25]	s	Cu(NCS)$_2$
	Le et al.[26]	non-s	Cu[N(CN)$_2$]Br, Cu(NCS)$_2$
surface impedance	Dressel et al.[27]	s	Cu[N(CN)$_2$]Br, Cu(NCS)$_2$
	Achkir et al.[28]	non-s	Cu(NCS)$_2$
magnetization	Lang et al.[29]	s	Cu(NCS)$_2$
	Lang et al.[30]	s	Cu[N(CN)$_2$]Br
	Specific Heat		
	Nakazawa et al.[31]	non-s	Cu[N(CN)$_2$]Br
	Elisinger et al.[32]	s	Cu[N(CN)$_2$]Br
	Kovalev et al.[33]	s	Cu(NCS)$_2$
	Mukker et al.[34]	s	Cu(NCS)$_2$
	STS		
	Arai et al.[35]	non-s	Cu(NCS)$_2$
	Thermal Conductivity		
	Belin et al.[36]	non-s	Cu(NCS)$_2$
	Izawa et al.[37]	non-s	Cu(NCS)$_2$
	Millimeter-Wave Transmission		
	Schrama et al.[38]	non-s	Cu(NCS)$_2$

the pairing. In this section, ^{13}C NMR studies on superconductivity in κ-Cu(NCS)$_2$ and κ-Cu[N(CN)$_2$]-Br are described.

There are two local-field components which the nuclei see in the superconducting state under magnetic field. One is from the thermally activated quasiparticles, and the other is from vortices. The latter one is further divided into the core-induced quasiparticle contribution and the spatial /temporal field fluctuations of flux quanta. In principle, we have two ways to use NMR for probing the nature of electron pairing: (i) examining the temperature dependence of the relaxation rate and the Knight shift, which reflect the thermally activated quasiparticles, and (ii) observation of the spatial profile of the vortex core. Method ii is stimulated by research of the cuprates but still remains challenging. To date, the organics have been investigated by method i, where the vortex contribution to shift and relaxation rate needs to be eliminated. In layered superconductors modeled by the Josephson-coupled superconducting multilayers, this is attained by applying the magnetic field parallel to the layers. Before presenting the data in this field condition, we show the data for the NMR relaxation rate under the perpendicular magnetic field in order to see the vortex contribution. Figure 14a shows the temperature dependence of $1/(T_1T)$ at three different sites (central ^{13}C, outer ^{13}C, and ^{1}H sites) in BEDT-TTF, as shown in Figure 14b. The applied magnetic field is 1.5 T perpendicular to the layer. The value of $1/(T_1T)$ is normalized to the values of the normal metallic state above T_C, where the relaxation is wholly due to quasi-particles. Therefore, even in the superconducting state, the quasiparticle contributions to the normalized $1/(T_1T)$ should

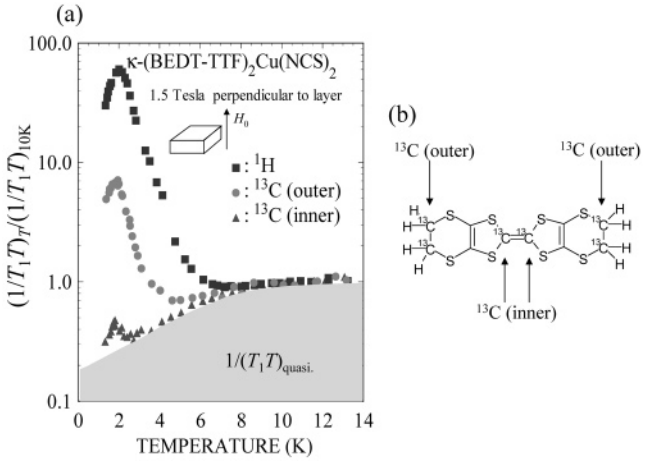

Figure 14. (a) Temperature dependence of $1/(T_1T)$ of a single-crystal κ-(BEDT-TTF)$_2$Cu(NCS)$_2$ at selective ^{13}C and ^{1}H sites (see part b) under fields perpendicular to the conducting layer. The shaded part expresses a quasiparticle contribution.

be the same at all three sites. The observed site-dependent variation of the behaviors below T_C is an indication of the other contribution, namely the field fluctuations of flux quanta, and its strong site dependence. In the order of the central ^{13}C, outer ^{13}C, and ^{1}H sites, the hyperfine coupling to the quasiparticles is weaker, while the flux fluctuations contribute to $1/(T_1T)$ at all sites equally. Therefore, the excess contributions in $1/(T_1T)$ normalized to the quasi-particle contribution are due to the dynamics of flux quanta. This contribution is seen to have a peak around 2 K, where the vortex liquid−solid transition is considered to occur. Although this contribution is appreciable as a small peak even in the central ^{13}C sites, the primary contribution is the quasi-particle relaxation, which is shown by the shaded region in Figure 14a.

Thus, the NMR experiment at the central ^{13}C sites is the best way to probe the pairing symmetry. In this field configuration, however, most of the quasiparticles are in the vortex core. To remove the core-induced contribution, the magnetic field is aligned parallel to the layers so that the Josephson votices are locked between the layers without core penetration into the layers. As the ^{1}H NMR relaxation rate is a sensitive probe of the vortices, as seen above, we used ^{1}H NMR to find the lock-in field condition. The experiment was performed for κ-Cu(NCS)$_2$. The angular dependence of $1/^1T_1$ at the ^{1}H site at 5 K is shown in Figure 15. The $1/^1T_1$ is constant away from the just parallel condition. In the field dependence of $1/^1T_1$ with the applied field perpendicular to the superconducting layer,[39] $1/^1T_1$ is reported to be insensitive to the density of pancake vortices in the vortex lattice state. In the present field geometries near the parallel configuration, the pancake vortex density is small in the lattice state. Thus, $1/^1T_1$ is reasonably insensitive to the field angle, which varies the pancake vortex density. With field approaching the parallel geometry, $^1T_1$ becomes gradually large and shows a steep increase. The longest $^1T_1$ remains in a narrow range of angle within $\pm 0.12°$ where the pancake vortices are considered to disappear. Ac-

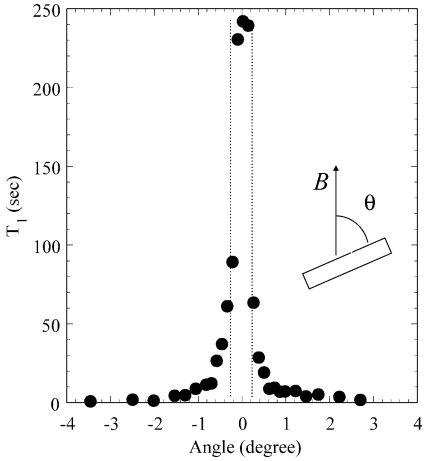

Figure 15. Angular dependence of the nuclear spin−lattice relaxation time at the ^{1}H site of κ-(BEDT-TTF)$_2$Cu(NCS)$_2$ under a field of 3.5 kOe and at 5 K.

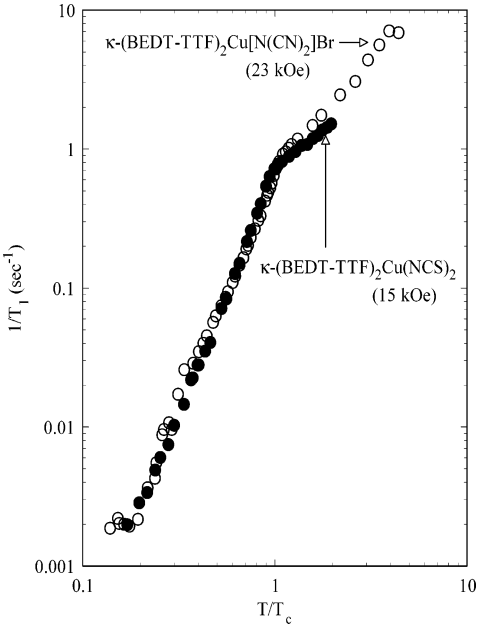

Figure 16. Temperature dependence of $1/T_1$ at the ^{13}C site for single-crystal κ-Cu[N(CN)$_2$]Br and κ-Cu(NCS)$_2$ plotted as a function of T/T_C.

cording to the simple model, where the lock-in state is realized when the perpendicular component of the external filed is lower than H_{c1}, the condition of the lock-in state turns out to be $H_{c1} < H \sin\theta$, where θ is the angle between the external field and the superconducting layer. Namely, the lock-in angle, θ_L, is given by $H_{c1} = \mathrm{H} \sin\theta_L$. Using a value of H_{c1} of 15 Oe as H_{c1},[40] we obtained $\theta_L = 0.15°$. $2\theta_L$ (= 0.3°) is in good agreement with the observed value of 0.25°.[40] So, we conclude that the vortex lock-in state is realized in this narrow range of angle. Then, we proceeded to measure $1/^{13}T_1$ at the ^{13}C site at a field of 15 kOe adjusted to the lock-in condition.

The temperature dependence of $1/^{13}T_1$ is shown in Figure 16. In general, $1/T_1$ is proportional to γ_n^2. The γ_n of ^{1}H is about 4 times as large as that of ^{13}C, so that T_1 at the ^{1}H site should be 16 times shorter than that at the ^{13}C site under the same field fluctuations. Using the value of $^1T_1 \sim 250$ s, the vortex motion component of $1/^{13}T_1$ at 4.5 K is expected to be 0.000 25 s^{-1}, which is negligible compared with the observed $1/^{13}T_1$ value of 0.01 s^{-1} at 4.5 K, which supports that the observed $1/^{13}T_1$ is governed by the thermally excited quasi-particle. The conventional s wave pairing has two distinctive features in the relaxation rate: (i) it should show an increase just below T_C and form the Hebel−Slichter coherence peak, and (ii) at low temperatures it should decrease, following an exponential function of temperature due to the gap opening in the quasi-particle excitation. The experimental data have neither of the characteristics; $1/^{13}T_1$ decreases below T_C without enhancement and follows a T^3 law at low temperatures. Both features strongly suggest the existence of line nodes in the gap parameter on the Fermi surface. The superconducting state is likely to be of non-s wave in nature, although the strongly anisotropic s wave state, where the size of the minimum gap is smaller than the thermal energy at the lowest temperature in this study (1.5 K), cannot be ruled out. In Figure 16, the $1/^{13}T_1$ of κ-Cu[N(CN)$_2$]Br is also plotted with $1/^{13}T_1$ and T normalized at T_C.[41] It is obvious that there is no difference between the two salts. The κ-Cu[N(CN)$_2$]Br was also studied at higher fields up to 78 kOe by Mayaffre et al.[12] and at a low field of 6 kOe by Soto et al.,[13] whose results are consistent with the present one.

Figure 17a shows the temperature dependence of ^{13}C spectra of κ-Cu(NCS)$_2$. From the spectral profile, the field is inclined about 40−50° from the a-axis in the ac-plane. The distribution of the lines above T_C comes from nonequivalent carbon sites with different Knight shifts. Below T_C, they move and merge around 120 ppm, which is nearly the chemical shift as observed for the neutral BEDT-TTF molecules in Figure 17a. This indicates that the spin susceptibility decreases below T_C. The temperature dependence of the first moment of the spectra is shown in Figure 17b. This behavior is clear evidence of the spin-singlet state in the superconducting state. A similar Knight shift profile is reported for κ-Cu[N(CN)$_2$]Br.[12,13,41]

All these NMR results suggest that the superconductivity is of d wave nature. Although there is controversy on the pairing symmetry in other experimental probes, NMR experiments have no controversy between the consequences of the three independent research groups.[12,13,41]

The mechanism of the electron pairing has long been discussed to be molecular vibration-mediated, lattice-phonon-mediated, or purely electronic.[8] Paying attention to the fact that the superconductivity appears in compounds containing molecules with the TTF structure, some specific molecular vibration was proposed to be responsible for the occurrence of superconductivity.[8,42] Actually, the analysis of the optical data suggests that the former two couplings are enhanced in BEDT-TTF compounds.[43] On the other hand, the fact that the superconducting phase abuts on the antiferromagnetic phase suggests the possible involvement of antiferromagnetic spin fluctuations in the superconductivity. Theoretical investigations along this line have been intensive.[44−48] We cannot make a decisive assessment on the proposals. However, it is mentioned that the pairing symmetries

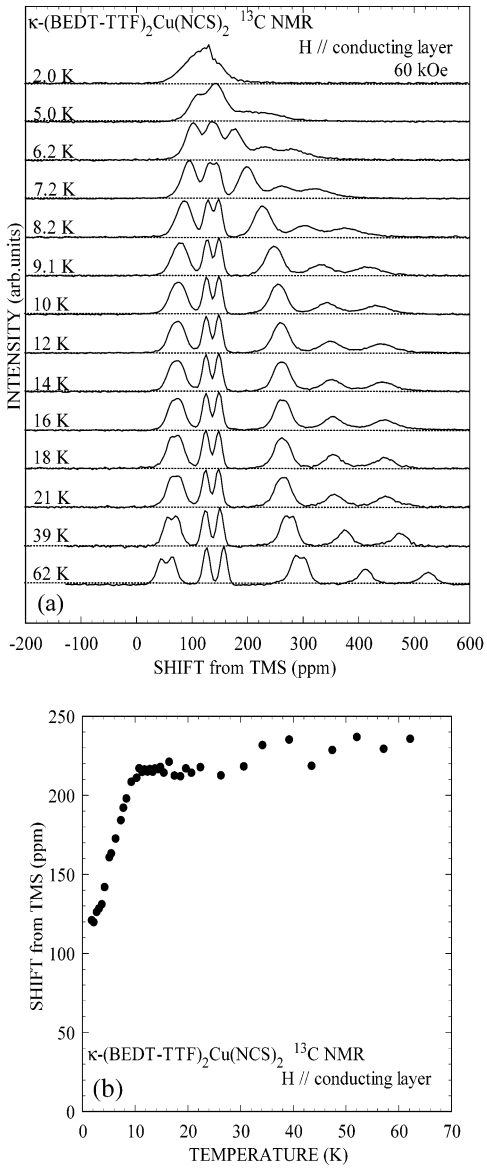

Figure 17. Temperature dependence of (a) the ^{13}C NMR spectra and (b) the NMR shift defined by its first moment for a single-crystal κ-Cu(NCS)$_2$ under a magnetic field of 60 kOe parallel to the layer.

deduced from the present NMR experiments are compatible with the consequence of the spin fluctuation-mediated model. There is a theoretical proposal to explain the neighboring superconductor and antiferromagnet in the phase diagram (Figure 3) on the same footing.[49]

5. Antiferromagnetic State

As presented in section 3, we observed the magnetic ordering in a powdered specimen of the Mott insulator, κ-Cu[N(CN)$_2$]Cl, by ^{13}C NMR measurements. In this section, we describe ^{1}H and ^{13}C NMR and magnetization measurements on a single-crystal sample for detailed characterization of the low-temperature magnetic structure, which was not determined in the experiments for the powder.

First, the ^{1}H NMR results are presented. Since the hyperfine field at the ^{1}H site is much smaller than that at the ^{13}C site due to the small spin density

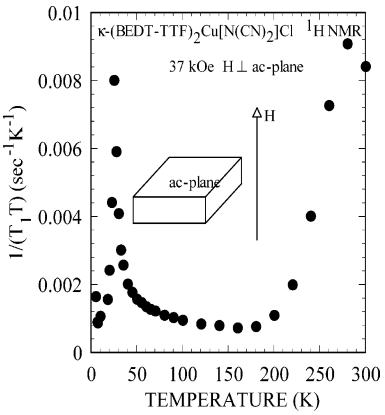

Figure 18. Temperature dependence of $1/(T_1T)$ at the ^{1}H site for a single-crystal κ-Cu[N(CN)$_2$]Cl under a magnetic field of 37 kOe perpendicular to the conducting layer. (Reprinted with permission from ref 50. Copyright 1995 American Physical Society.)

there, the whole ^{1}H NMR spectrum is within the frequency range covered by the radiofrequency (rf) pulse even in the magnetically ordered state. The nuclear spin−lattice relaxation rate and the spectra at the ^{1}H site were measured under a field of 37 kOe perpendicular to the conducting layer. The spectra were obtained by fast Fourier transform (FFT) of the echo signal, which was acquired by the pulse sequences of solid-echo $((\pi/2)x-(\pi/2)y)$ and spin−echo $((\pi/2)x-(\pi)x)$ above and below the magnetic transition, respectively, where x and y stand for the axes in the rotational frame. Figure 18 shows the temperature dependence of $1/(T_1T)$ at the ^{1}H site.[50] A steep increase above 200 K and a peak formation around 280 K are not of electronic origin but attributed to thermally activated vibration of the ethylene groups located at the edges of BEDT-TTF molecules. Since the motional contribution to $1/(T_1T)$ vanishes with an exponential function of temperature, $1/(T_1T)$ below 160 K is considered to be dominated by the electronic contribution. From the Blembergen−Purcell−Pound analysis of the motional contribution to T_1^{-1}, which is deduced by subtracting the electronic contribution extrapolated from the data below 160 K, an activation energy of the vibration is estimated at 2600 ± 100 K.

Below 160 K, $1/(T_1T)$ shows a gradual increase, which becomes steeper at lower temperatures. At 26−27 K, a sharp peak indicating the magnetic transition was observed, as in ^{13}C NMR (see section 3). This transition is confirmed to be antiferromagnetic, as described below. The value of $1/(T_1T)$, for example, 0.001 s^{-1} K^{-1} at 100 K, is near the values for the superconducting salts, κ-Cu(NCS)$_2$[51] and κ-Cu[N(CN)$_2$]Br,[52] which do not show magnetic order. This is consistent with the ^{13}C NMR results (section 3), which show common antiferromagnetic fluctuations among the salts at high temperatures above 60 K.

Figure 19 shows the temperature dependence of the ^{1}H NMR spectra.[50] The line width in the temperature range between 165 and 30 K is reasonably explained by the nuclear dipole coupling between the protons in the ethylene groups. Below 27 K, the spectra split into three lines, which indicates generation of an inhomogeneous local field at the ^{1}H site.

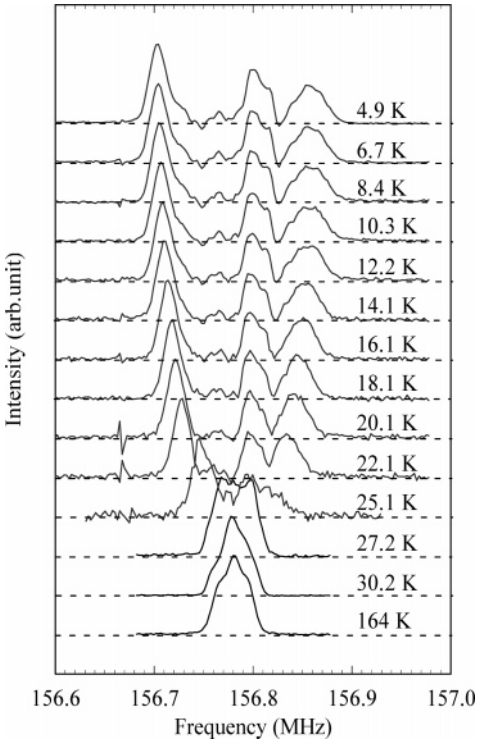

Figure 19. ^{1}H NMR spectra of a single-crystal κ-Cu[N(CN)$_2$]Cl at a field perpendicular to the *ac*-plane (conducting plane) at different temperatures. (Reprinted with permission from ref 50. Copyright 1995 American Physical Society.)

We can extract two consequences on the ordered state from the observed spectra. One is on the magnetic structure. If the antiferromagnetic order is incommensurate with the lattice, distribution of the local field at ^{1}H sites should be continuous, and broad NMR spectra are expected. However, the observed spectra have a discrete nature. This provides an evidence for a commensurate magnetic structure. The other is on the moment of the antiferromagnetic order. The splitting width from the center is $\pm$80 kHz, which corresponds to the local filed of $\pm$20 G at the ^{1}H sites. As the spin flop field is lower than the NMR measurement field, as described below, the ordered moments should be flopped in a direction perpendicular to the external filed. Since the shift of the line is proportional to the local field component parallel to the applied field, the isotropic term of the hyperfine tensor does not contribute to the line splitting, but the anisotropic term which comes from the dipole field of the localized spins is responsible for the line splitting. Using the spin density profile of the highest occupied molecular orbital (HOMO) of BEDT-TTF calculated by the extended Huckel method,[53] we can estimate the parallel component of the local field at each ^{1}H site from the one-electron spin on BEDT-TTF. The ordered moment is estimated at 0.4$-$1.0 μ_B/dimer.

To confirm the spin structure and estimate the moment, we measured the ^{13}C NMR spectra below 100 K in a field of 80 kOe perpendicular to the conducting layer.[54] Figure 20 shows the ^{13}C NMR spectra of κ-Cu[N(CN)$_2$]Cl. In the paramagnetic state at high temperatures, the spectra are composed of two peaks from the neighboring two ^{13}C sites with

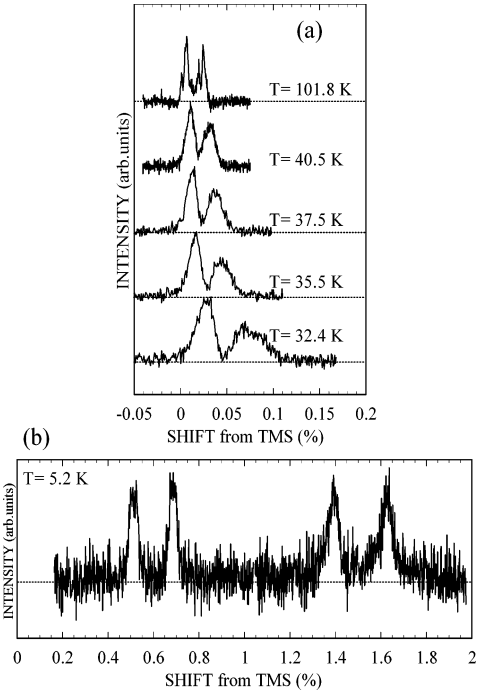

Figure 20. ^{13}C NMR spectra of a single-crystal κ-Cu[N(CN)$_2$]Cl under a field perpendicular to the layer above T_N (a) and at 5.2 K < T_N 27 K (b). (Reprinted with permission from ref 54. Copyright 2000 Elsevier.)

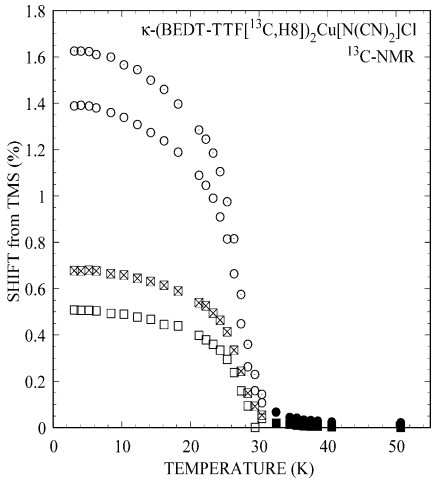

Figure 21. Temperature dependence of the peak positions of ^{13}C NMR spectra for κ-Cu[N(CN)$_2$]Cl. This indicates growth of the sublattice moment.

different shifts. At 100 K, one can appreciate splitting of each line due to the nuclear dipolar coupling. When temperature is decreased toward T_N, the spectra are gradually shifted and broadened. This indicates the growing short-range order. Below T_N, the four discrete lines, which clearly indicate a commensurate magnetic structure, appear as seen in the spectrum at 5.2 K. The temperature dependence of the peak positions, which indicates growth of the sublattice moment, is shown in Figure 21. The spectral shift is one-sided, and there is no signal in a negative frequency range (not shown in Figure 20). As will be shown by the magnetization measurements below, the easy axis of the antiferromagnetic order is perpendicular to the conducting layer but, in the present field condition, the spin should be flopped

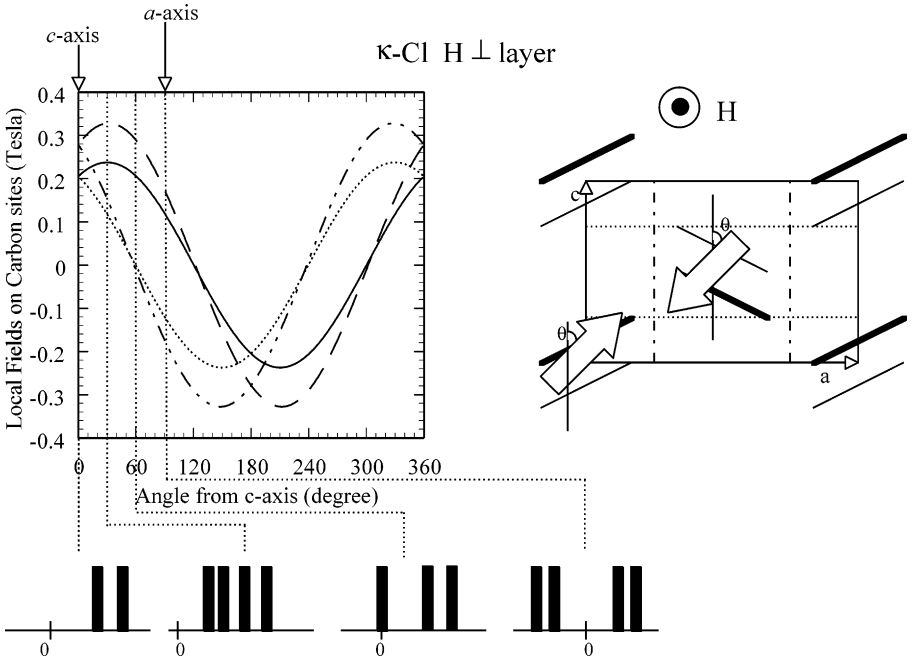

Figure 22. Simulated angular dependence of the peak positions of ^{13}C NMR spectra against in-plane rotation of the antiferromagnetic spin under a field perpendicular to the plane.

parallel to the conducting plane. We simulated the NMR spectra for the antiferromagnetically ordered dimer spins against the in-plane spin rotation with the spins kept flopped, assuming the hyperfine shift tensor of κ-Cu[N(CN)$_2$]Br.[13] The simulated angular dependence of the peak positions is shown in Figure 22. The observed line profile at 5.2 K is reproduced by an about 30° orientation of the local moment of 0.45 μ_B on a dimer against the a-axis. [More rigorous analysis of the ^{13}C NMR spectrum for determination of the spin structure is given in section 6.] This value is consistent with the result of ^{1}H NMR.

These features indicate that the ordered state in κ-Cu[N(CN)$_2$]Cl is in contrast to the SDW state of (TMTSF)$_2$PF$_6$. The ^{1}H NMR study on (TMTSF)$_2$PF$_6$ revealed the incommensurate nature of the magnetic order, which is explained by nesting of the Fermi surface.[55] On the other hand, the commensurate ordered state in κ-Cu[N(CN)$_2$]Cl is understood as a ground state of a Mott insulator. The Fermi surfaces predicted by band structure calculations[56] do not have a suitable shape for nesting.

As described in section 3, the susceptibility of κ-Cu[N(CN)$_2$]Cl suggests the presence of weak ferromagnetism.[16] To see the magnetic structure in further detail, the magnetization was measured for the single crystal, which was used in the ^{1}H NMR measurements.[50] Figure 23 shows the temperature dependence of susceptibility at different magnitudes and configurations of the external field. At 1 kOe, a large anisotropy is observed below 27 K (Figure 23a). The spin susceptibility is enhanced when the external filed is parallel to the conducting layer, while it is suppressed under perpendicular field. This fact shows that a weak ferromagnetic component is oriented in the ac-plane. At 10 kOe, the enhancement of susceptibility is observed in both field directions, although the anisotropy still remains (Figure 23b). Figure 24 shows magnetization curves in a different orientation

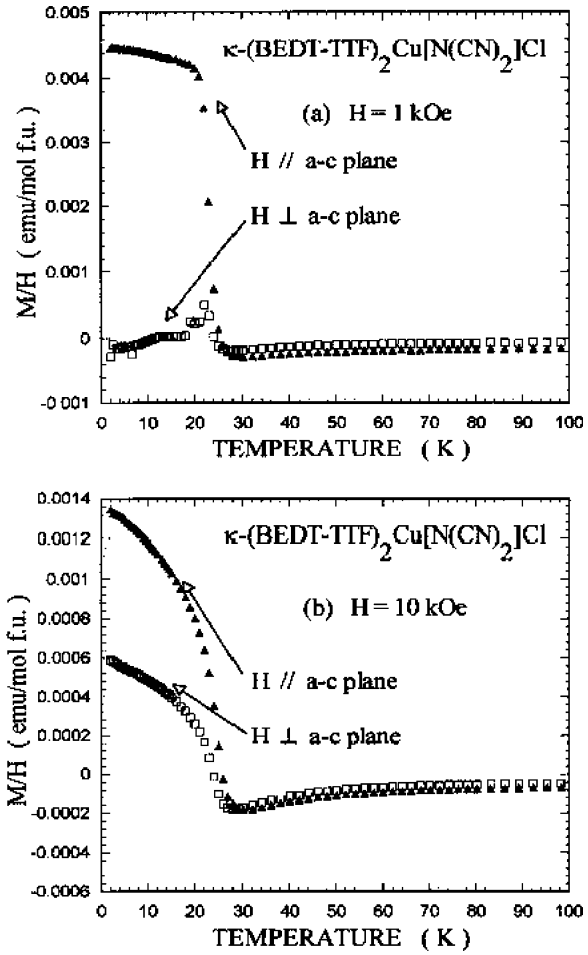

Figure 23. Temperature dependence of the susceptibility for κ-Cu[N(CN)$_2$]Cl under different field configurations at 1 kOe (a) and 10 kOe (b). (Reprinted with permission from ref 50. Copyright 1995 American Physical Society.)

of the magnetic field against the crystal. The field dependence of the magnetization is linear at 27 K,

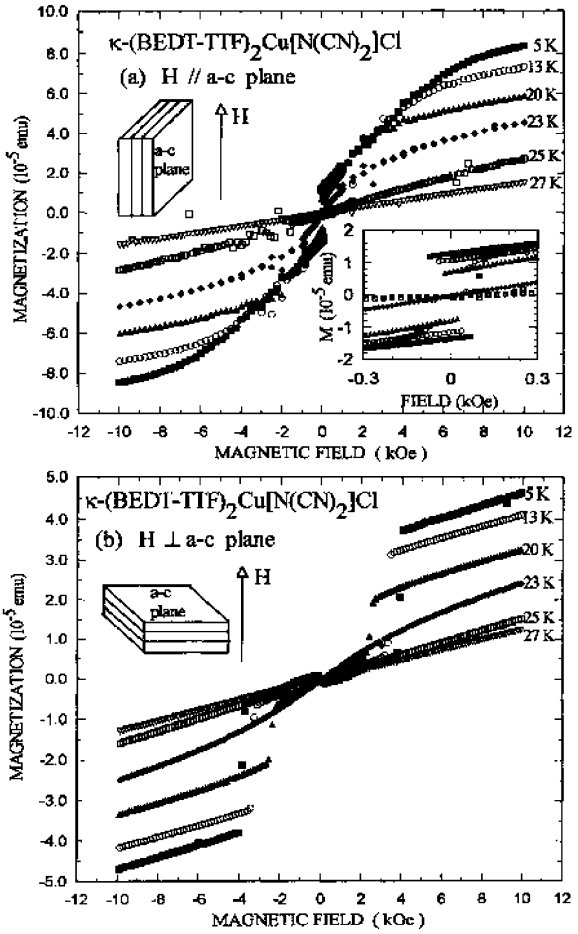

Figure 24. Magnetization vs external field for κ-Cu[N(CN)$_2$]Cl under magnetic fields parallel (a) and perpendicular (b) to the conducting plane. (Reprinted with permission from ref 50. Copyright 1995 American Physical Society.)

where the antiferromagnetic transition occurs. At lower temperatures, clear hystereses are observed below 23 K in a parallel field (Figure 24a). As described above, ^{1}H and ^{13}C NMR reveal that the magnetic transition at 27 K is antiferromagnetic. Therefore, it is reasonable to conclude that the origin of the weak ferromagnetism comes from the spontaneous canting of the antiferromagnetically aligned moments. Considering that the canting direction is parallel to the *ac*-plane, the easy axis of the antiferromagnetic spins is perpendicular to the *ac*-plane. This is confirmed by the external field dependence of magnetization in the perpendicular configuration (Figure 24b). Below the transition temperature, the magnetization shows a discontinuous jump at a field depending on temperature. It is explained by the occurrence of the spin flop, which suggests that the easy axis is perpendicular to the conducting plane. This is consistent with the magnetization behavior under the parallel-field configuration.

From these results, we summarize the profile of the magnetic transition and structure in κ-Cu[N(CN)$_2$]Cl as follows: Below 26−27 K, the compound undergoes an antiferromagnetic phase transition to a commensurate spin structure of 0.45 μ_B on a dimer. The easy axis is perpendicular to the conducting layer, but the spins are canted parallel to the layer.

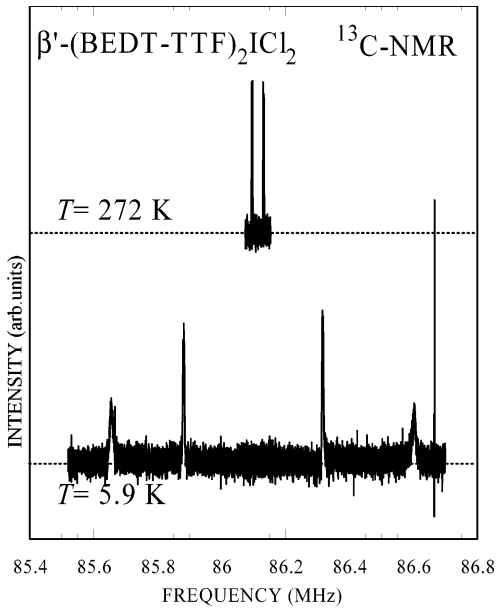

Figure 25. ^{13}C NMR spectra for a single-crystal β'-(BEDT-TTF)$_2$ICl$_2$ at room temperature and 5.9 K, which is below the antiferromagnetic transition at 25 K.

Judging from the magnitude of the ferromagnetic component, the canting angle is so small that the spins are nearly antiparallel in a direction normal to the layers. This spin configuration is consistent with the detailed analysis of the single-crystal ^{13}C NMR spectra by Smith et al.[57] and the magnetic anisotropy study by Pinteric et al.,[58] who both showed the importance of the Dzialoshinskii−Moriya interaction in this type of spin ordering.

As shown in Figure 3, β'-(BEDT-TTF)$_2$ICl$_2$ is regarded as a Mott insulator with a larger *U*/*W* than that for κ-(BEDT-TTF)$_2$X. This comes from strong dimerization in β'-(BEDT-TTF)$_2$ICl$_2$. Actually, the charge gap deduced from the temperature dependence of the resistivity is estimated at 120 meV,[59] while that of κ-Cu[N(CN)$_2$]Cl is ∼50 meV at low temperature. We also examined the spin structure of this salt through observation of the ^{13}C NMR spectra. Since all BEDT-TTF molecules in the β' arrangement are equivalent against any direction of magnetic field, ^{13}C NMR spectra are simple, as shown in Figure 25. The spectrum at 272 K consists of two lines coming from the two neighboring ^{13}C═^{13}C with different shift tensors. (Each line is a Pake doublet which is not resolved in the scale of Figure 25.) Below the antiferromagnetic transition at 22 K, each line is clearly split into two lines on the positive and negative sides, giving totally four lines. This spectrum is easily understood by the commensurate spin structure as in κ-Cu[N(CN)$_2$]Cl. The difference of the splitting profile between the two salts (only positive shits in κ-Cu[N(CN)$_2$]Cl versus bipolar shifts in β'-(BEDT-TTF)$_2$ICl$_2$) results from the difference of the dimer arrangement; up and down spins are located on the nonequivalent dimers in the former while they are on the equivalent dimers in the later (see section 6). Assuming the ^{13}C hyperfine tensors of κ-Cu[N(CN)$_2$]Br,[13] the ordered moment is estimated at 0.30 μ_B/dimer. This salt has no spin canting.[60]

6. Electronic State on the Border of the Mott Transition

As described in section 3, the fully deuterated κ-(BEDT-TTF)$_2$Cu[N(CN)$_2$]Br (κ-d[4,4]-Cu[N(CN)$_2$]-Br) is revealed to be situated just on the metal−insulator boundary by the ^{13}C NMR, ^{1}H NMR, and susceptibility measurements for the powdered sample.[18] In this section, we present the results of the single-crystal ^{13}C NMR experiments of κ-d[4,4]-Cu[N(CN)$_2$]Br, which clarify the nature of the metallic/superconducting phase and the Mott insulating phase residing on the Mott border.[61]

An external filed of 80.3 kOe was applied parallel to the a-axis, which is parallel to the conducting ac-plane of κ-d[4,4]-Cu[N(CN)$_2$]Br. In this field geometry, the ^{13}C NMR spectral splitting due to the nuclear dipole coupling vanishes because this particular angle between the external field and the ^{13}C=^{13}C direction forms the "magic angle", as found for κ-d[0,0]-Cu[N(CN)$_2$]Br by De Soto et al.[13] Moreover, all of the BEDT-TTF molecules become equivalent against the field parallel to the a-axis. So, only two NMR lines coming from the two neighboring ^{13}C sites with different Knight shift are expected to be observed. The observed spectra are shown in Figure 26a and b.[61] At higher temperatures, the spectra consist of two peaks (line A with a smaller shift and line B with a larger shift), as expected. At low temperatures below 20 K, the spectra from the magnetic insulating phase are separated from the metallic (or superconducting) phase spectra, as seen in Figure 26b. [Note the difference of the shift scales of parts a and b of Figure 26.]

With decreasing temperature, the spectra show the steplike broadening around 150 K, and further gradual broadening starts below 70 K, as seen in the temperature dependence of the line width for lines A and B plotted in Figure 26c. The broadening is also observed in κ-d[0,0]-Cu[N(CN)$_2$]Br[12,13,39] and likely has something to do with the superlattice formation revealed by XRD,[62] although it is still not clear. In κ-d[0,0]-Cu[N(CN)$_2$]Br, the line broadening levels off around 50 K, where the nonmetal−metal crossover occurs.[13] However, the line broadening for κ-d[4,4]-Cu[N(CN)$_2$]Br is developed down to 32 K. This is considered as the manifestation of the growing antiferromagnetic short-range order. Then, the complicated line shapes are observed around 30 K and the spectra split into two components in quite different frequency regions at low temperatures: one stays in the shift range of Figure 26a, while the other component begins to be out of the range of Figure 26a below ~20 K and shows a huge shift of percent order at low temperatures, as seen in Figure 26b. This huge shift indicates the generation of a local field due to the magnetic ordering. The two spectral components separated below 30 K are from the metallic phase, which undergoes the superconducting phase transition at 11 K (see below), and from the insulating phase, which undergoes the antiferromagnetic transition at 15 K (see below). These facts indicate that the system enters into a two-phase regime associated with the first-order character of the Mott transition driven by physical or chemical pressure. It is seen in Figure 26a that separation in line A occurs with comparable intensity at 29.3 and 27.3 K, meaning that the separated phases have comparable volume fractions at these temperatures. The two-phase spectra become so well separated below 15 K that the relative intensity of the antiferromagnetic phase can be evaluated and is found to increase from 60% at 15.2 K to 85% at 5.7 K. The increasing volume fraction of the insulating phase at lower temperatures is consistent with the inclined Mott transition line in the temperature−pressure phase diagram of κ-Cu[N(CN)$_2$]Cl.[20,63−65]

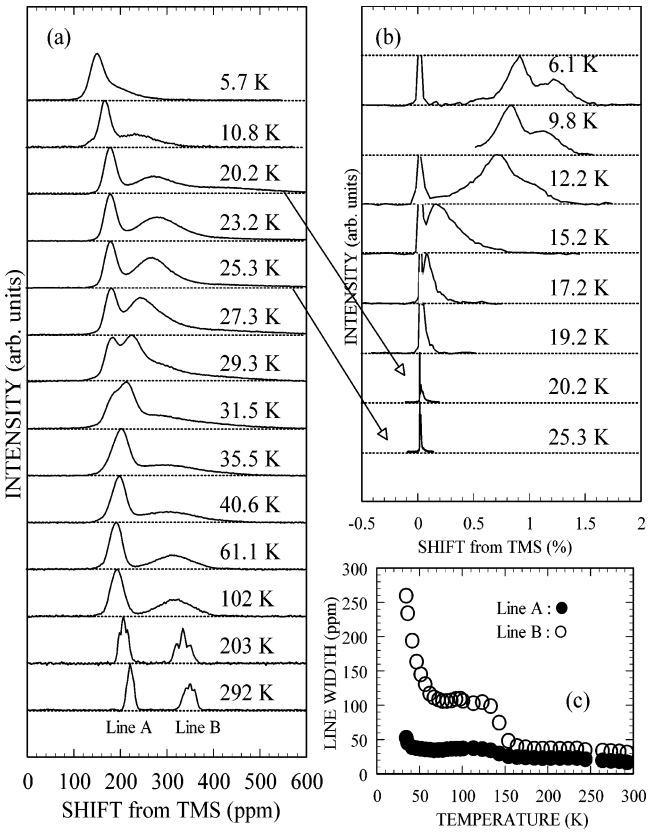

Figure 26. ^{13}C NMR spectra of the single-crystal κ-d[4,4]-Cu[N(CN)$_2$]Br in shift ranges of hundreds of ppm (a) and of percent (b).[53] (c) Temperature dependence of the line width above 30 K. The magnetic field was applied perpendicular to the conducting layer. (Reprinted with permission from ref 61. Copyright 2002 American Physical Society.)

As seen in Figure 26b, the ^{13}C NMR spectrum of the antiferromagnetic phase at the lowest temperature has two distinct features, which give a key to solve the spin structure. The first one is the doubly peaked structure. The second one is the spectral shift only to the positive frequency side by ~1%, which corresponds to ~0.9 MHz. We confirmed that there was no signal on the negative frequency side down to −2%, which corresponds to −2 MHz. These features are in strong contrast to the case of the nesting-driven incommensurate SDW, where the spectra have a continuous U-shaped distribution around the origin of the shift, as observed in (TMTSF)$_2$PF$_6$.[66] The present result shows a commensurate magnetic structure similar to the case of κ-Cu[N(CN)$_2$]Cl described in section 5. For determination of the spin structure, we review the crystal structure, which restricts the possible spin configurations. The struc-

tural symmetry of κ-d[4,4]-Cu[N(CN)$_2$]Br is *Pnma*, where all the BEDT-TTF molecules are equivalent in crystallography. Since the inversion symmetry is at the center of the BEDT-TTF dimer, two molecules in the dimer are equivalent against any field direction. Therefore, if the spins were antiparallel in the dimer, the spectra would be split into positive and negative frequency sides according to the opposite hyperfine field. The one-sided shift in Figure 26 rules out this spin alignment. Furthermore, keeping of the double peaked structure below the Neel temperature indicates that the magnitude of the local moment is the same on all the molecules because one BEDT-TTF molecule gives two lines. Namely, the spin is parallel and equally populated on both molecules in a dimer. This supports the dimer model where the system is described by a lattice of dimers without internal electronic degrees of freedom, as described in section 1. The NMR shift is proportional to the field-parallel component of the local field. At first sight, the one-sided shift seems to give an indication of ferromagnetic spin structure. However, it is not so straightforward, because the hyperfine shift tensors at the ^{13}C sites are anisotropic and there are two differently oriented dimers (dimer-I and dimer-II). What the experimental result indicates is that the *a*-axis component of the hyperfine field from the local moment is the same for all the molecules. Its first-hand consequence is that the dimer spin is ferromagnetic within the dimer-I sublattice and the dimer-II sublattice. The question is the configuration between the two sublattice moments.

According to the symmetry of *Pnma*, dimer-I and dimer-II are connected by the *ab*-plane mirror operation with *a*-axis translation. By this operation of the local spin on a dimer, the *a*-axis and *b*-axis components of the dimer spin and hyperfine field are unchanged while the *c*-axis component is reversed. Considering this characteristic of the mirror operation, the dimer spin configurations to give the same *a*-axis component of the hyperfine field are restricted to the following three types, as shown in Figure 27, where the spectral profiles calculated with use of the hyperfine coupling tensors[13] are also shown: (i) ferromagnetic alignment directed to the *a*-axis (Figure 25a); (ii) ferromagnetic alignment directed to the *b*-axis (Figure 27b); (iii) antiferromagnetic dimer spin structure parallel to the *c*-axis (Figure 27c).[61] The magnetic susceptibility of this salt shows a very weak temperature dependence down to about 100 K and gradually decreases down to 15 K, where a sudden increase was observed due to the appearance of weak ferromagnetism (section 5). This behavior indicates that the in-plane exchange coupling between spins is not ferromagnetic but antiferromagnetic (section 5). Thus, spin configurations i and ii are ruled out. Indeed, in the case of i, the spectral shift is determined by the diagonal part of the hyperfine tensors (*a*,*a*), which is more than three times different for the neighboring carbon sites.[13] This ratio contradicts the observed shift ratio of the two lines that is 1.5. We also calculated the local field assuming the flopped antiferromagnetic spin structure within the *bc*-plane. It is seen in Figure 28 that this spin

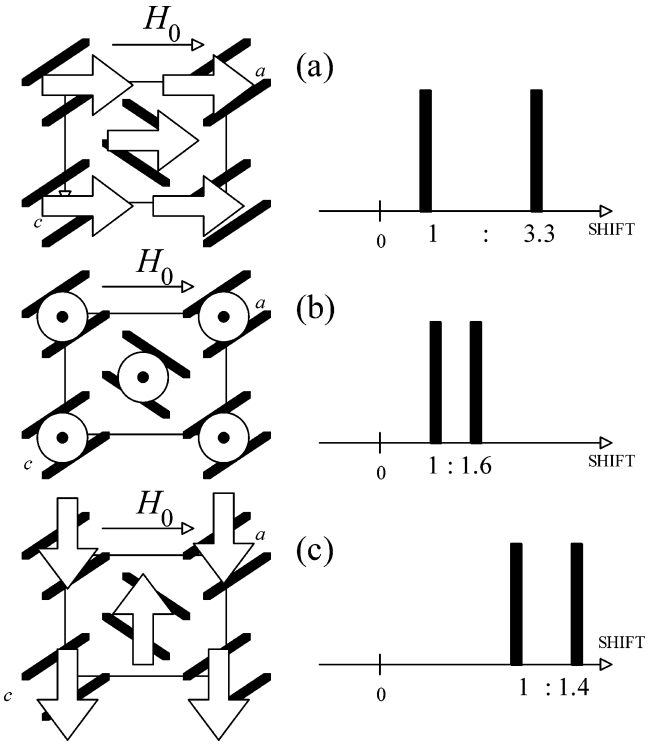

Figure 27. Possible spin configurations (left) and calculated spectral profiles (right) under a field parallel to the *a*-axis for explanation of the one-sided shift of spectra below the Neel temperature. (Reprinted with permission from ref 61. Copyright 2002 American Physical Society.)

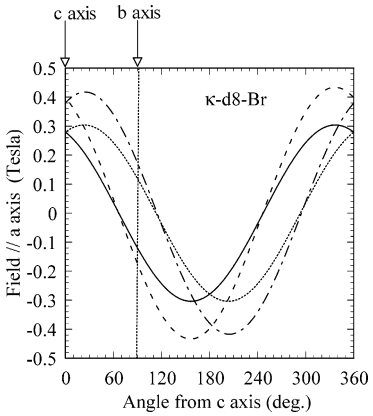

Figure 28. Simulated angular dependence of peak positions of ^{13}C NMR spectra against *bc*-plane (perpendicular to the conducting plane) rotation of the antiferromagnetic spin under a field parallel to the *a*-axis.

direction is unique to give the two-line spectrum against spin rotation in the *bc*-plane. Moreover, the observed shift ratio of the two lines is 1.5, which is close to the simulated value of 1.4. Thus, the dimer spin is concluded to have the simplest antiferromagnetic configuration (iii), as depicted in Figure 27c. Under the present field of 80 kOe, the local spins should be flopped. Spin arrangement iii is consistent with the flopped configurations.

The amplitude of the ordered moment is estimated from the observed spectral shift and the hyperfine shift tensors reported by De Soto et al.[13] If a local moment of 1.0 μ_B stands on a dimer and is directed to the *c*-axis, the *a*-axis component of the hyperfine field for the site giving line A is 2.8 kOe, which

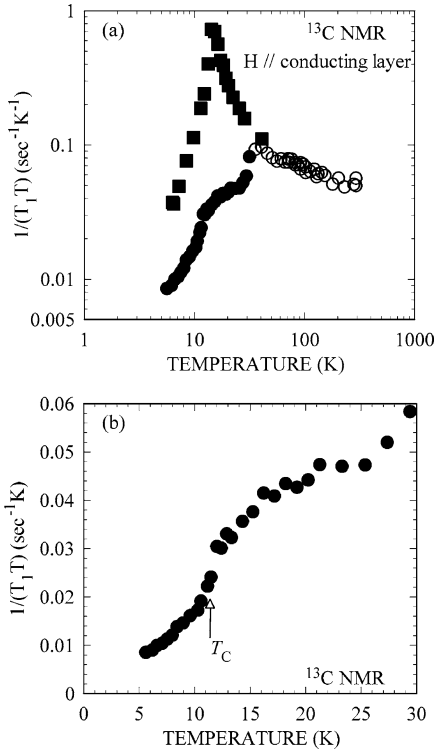

Figure 29. (a) Temperature dependence of $1/(T_1T)$ at the ^{13}C site of the superconducting (closed circles) and antiferromagnetic (closed squares) phases for the single-crystal κ-d[4,4]-Cu[N(CN)$_2$]Br below 30 K and of the high-temperature phase (open circles) above 30 K.[53] (b) Temperature dependence of $1/(T_1T)$ of the superconducting phase at low temperatures in linear scales. (Reprinted with permission from ref 61. Copyright 2002 American Physical Society.)

corresponds to a shift of 3.0 MHz. So, the observed shift of 0.78 MHz shows that the ordered moment of 0.26 μ_B/dimer stands on a dimer at 6.1 K. Another Mott insulator, κ-Cu[N(CN)$_2$]Cl, has a larger moment of 0.45 μ_B/dimer and a high Neel temperature, T_N, of 27 K (see section 5). These differences are reasonable, considering that κ-Cu[N(CN)$_2$]Cl is situated farther from the metal−insulator boundary than κ-d[4,4]-Cu[N(CN)$_2$]Br salt.

Figure 29a shows the temperature dependence of $1/(T_1T)$ of κ-d[4,4]-Cu[N(CN)$_2$]Br.[61] The T_1 was determined for line A. At low temperatures where the spectra from the magnetic insulating phase are separated from the metallic (or superconducting) phase spectra, the relaxation rate of the AF phase was determined at the peak position of the spectra. As temperature decreases, $1/(T_1T)$ is gradually increased in a manner similar to that for κ-d[0,0]-Cu[N(CN)$_2$]Br and κ-(BEDT-TTF)$_2$Cu[N(CN)$_2$]Cl. The common behaviors indicate the growing antiferromagnetic spin fluctuations. Owing to the separation of the spectra below 30 K due to the superconductor−antiferromagnetic insulator phase separation, $1/(T_1T)$ of each phase was obtained separately. The $1/(T_1T)$ of the insulating phase continuously increases below 30 K, implying that this phase is a low-temperature continuation of the high-temperature single phase, and forms a divergent peak indicating the magnetic order at around 15 K. The whole feature of $1/(T_1T)$ is the same as that for the Mott insulator, κ-Cu[N(CN)$_2$]Cl salt, except for the Neel temperature.

The other part of the spectrum observed in the range 100−300 ppm has contrasting behavior. Around 30 K, where the spectral separation occurs, $1/(T_1T)$ shows a steep decrease, meaning suppression of the antiferromagnetic spin fluctuations. It is also observed in κ-d[0,0]-Cu[N(CN)$_2$]Br around 45 K, which coincides with the inflection point of the metal−nonmetal resistivity crossover. The present result implies that the crossover temperature is decreased to 30 K for κ-d[4,4]-Cu[N(CN)$_2$]Br. It is also remarkable that $1/(T_1T)$ shows an anomalous decrease below 30 K, as seen in Figure 29b. Since the superconducting transition temperature of κ-d[4,4]-Cu[N(CN)$_2$]Br is 11 K,[5,18,67] it turns out that the decrease in $1/(T_1T)$ begins at much higher temperatures than T_C and becomes steeper as temperature approaches T_C. While such a tendency in $1/(T_1T)$ is also observed in κ-d[0,0]-Cu[N(CN)$_2$]Br, the feature is much more prominent in κ-d[4,4]-Cu[N(CN)$_2$]Br. The decrease is too steep to observe a clear kink associated with the superconducting phase transition. This behavior is reminiscent of the so-called pseudogapped behavior observed in the underdoped high-T_C cuprates.[68] Although its origin is still controversial, the present result can be addressed to the peseudogap, which may be of common nature to the cuprates. It is interesting that the bandwidth controlled organics and the band-filling controlled cuprates share one of the most mysterious features in the vicinity of the Mott transition. The sharpened nonmetal−metal crossover and the enhanced peseudogap characterize the metallic side of the Mott transition. Our recent experiments have revealed that the pseudogap behavior is strongly dependent on the magnitude and the angle of the magnetic field.

The separated two phases in κ-d[4,4]-Cu[N(CN)$_2$]-Br are extrapolations to the Mott boundary from the superconducting phase of κ-d[0,0]-Cu[N(CN)$_2$]Br and the antiferromagnetic insulating phase of κ-Cu-[N(CN)$_2$]Cl. From the present results, we conclude that the peseudogapped superconducting phase with T_C of 11 K abuts on the commensurate AF insulator with T_N of 15 K in the two-dimensional organic conductors. The fact that both phases have finite order parameters as measured by T_C, T_N, and the AF moment on the phase boundary means that the Mott transition is of the first order. Recent transport studies of κ-Cu[N(CN)$_2$]Cl under continuously controllable He gas pressure revealed that the Mott transition is of first-order and has a critical end point.

7. Concluding Remarks

Historically, the BEDT-TTF molecule attracted interest because it afforded many two-dimensional metals stable against the Fermi surface nesting, which was encountered in the quasi-one-dimensional systems such as TMTSF compounds. The synthesis of various kinds of BEDT-TTF salts has served deepening and cultivating physics of Fermi surface topology. At the same time, it has come to a common recognition that superconductivity with relatively high transition temperature has emerged in the family of κ-(BEDT-TTF)$_2$X. In this stream of research, this family was found to have an insulating member,

which gave researchers a chance to direct attention toward comprehension of the metal, superconductor, and insulator in light of electron correlation. The NMR study presented in this article is an attempt to tackle this issue from the experimental point of view. The NMR study of κ-(BEDT-TTF)$_2$X gave the following consequences:

(1) κ-(BEDT-TTF)$_2$X are strongly correlated electron systems with strong antiferromagnetic spin fluctuations, and metallic and insulating phases are understood in the context of the Mott transition.

(2) The superconductivity appearing in the metallic phase at low temperatures has the symmetry of d wave pairing.

(3) The antiferromagnetic order appearing in the insulating phase at low temperatures has a commensurate spin structure.

(4) The superconducting and antiferromagnetic phases abut on each other with the first-order transition.

(5) The metallic phase in the vicinity of the Mott transition is pseudogapped at higher temperatures above T_C.

Tentatively, these features can be addressed as common characteristics of the bandwidth-controlled Mott transition but should be examined in other families of materials.

As future problems to be explored in κ-(BEDT-TTF)$_2$X by NMR, we raise two issues. One is the criticality of the Mott transition. As suggested by the recent experiments on κ-Cu[N(CN)$_2$]Cl under continuously controllable He gas pressure, the first-order Mott transition has a critical end point in the temperature−pressure diagram.[63−65] NMR study around the critical point would be informative for the study of the critical phenomena of the correlated electron fluid.

The other one is on the frustration in the spin degree of freedom. As introduced in section 1, the conducting layer is modeled to the two-dimensional lattice of dimers with a half-filled band. As seen in Figure 1b, the dimer lattice forms the anisotropic triangular lattice characterized by two kinds of transfer integrals, t and t'. The systems, κ-Cu(NCS)$_2$, κ-Cu[N(CN)$_2$]Br, and κ-Cu[N(CN)$_2$]Cl, treated in this article have anisotropies, t'/t, of 0.84, 0.68, and 0.74, respectively. The antiferromagnetic order with a large magnetic moment in the Mott insulator, κ-Cu[N(CN)$_2$]Cl, is closely related to this anisotropy. Recently, another Mott insulator, κ-Cu$_2$(CN)$_3$, with a nearly isotropic triangular lattice ($t'/t \sim 1$) has been found to show no magnetic ordering.[69] The possible spin liquid state in the insulating phase is an intriguing topic in condensed matter physics. Moreover, under pressure this salt shows a Mott transition to the metallic state, which exhibits superconductivity at low temperatures.[70,71] This contrasts with the well-known feature that the superconducting phase neighbors the antiferromagnet, as in high-T_C cuprates;[72] the nature of superconductivity has been discussed in the context of possible involvement of the antiferromagnetic interaction. The superconductivity emerging in the spin liquid will give a new dimension to this problem. In the near future, NMR is expected to play a vital role in opening the experimental field to the physics of the Mott transition on the triangular lattice.

8. Acknowledgment

The authors are greatly indebted to E. Nomura, N. Yokoi, Y. Morita, K. Nakatsuji, T. Suzuki, and H. Anzai for preparation of ^{13}C-enriched molecules in starting up the ^{13}C NMR business of organic conductors. The authors are grateful to Y. Nakazawa, H. Taniguchi, K. Hiraki, H. Sato, and A. Shimizu for fruitful collaborations and to K. Kato, T. Takayama, K. Hayasaka, M. Sakai, S. Sato, and Y. Ohno for their support in low-temperature experiments. Helpful discussions with H. Fukuyama, H. Kino, K. Miyake, Y. Tokura, H. Seo, T. Mori, R. Kato, H. Kobayashi, A. Kobayashi, T. Takahashi, N. Nagaosa, S. Murakami, M. Imada, S. Onoda, S. Watanabe, C. Hotta, and V. Ivanov are gratefully acknowledged.

9. References

(1) Mori, T. *Bull. Chem. Soc. Jpn*. **1999**, *72*, 179.
(2) Kanoda, K. *Hyperfine Interact*. **1997**, *104*, 235.
(3) Ohshima, K.; Mori, T.; Inokuchi, H.; Urayama, H.; Yamochi, H.; Saito, G. *Phys. Rev. B* **1988**, *38*, 938.
(4) Kino, H.; Fukuyama, H. *J. Phys. Soc. Jpn.* **1995**, *64*, 2726.
(5) Taniguchi, H.; Kawamoto, A.; Kanoda, K. *Phys. Rev. B* **1999**, *59*, 8424. Taniguchi, H.; Kawamoto, A.; Kanoda, K. *Phys. Rev. B* **2003**, *67*, 014510.
(6) Kanoda, K. *Physica C* **1997**, *282−287*, 299.
(7) It is noted that the Mott critical value of *U*/*W* depends on the in-plane band structure anisotropy, as was suggested by: Hotta, C.; Fukuyama, H. *J. Phys. Soc. Jpn*. **2001**, *70*, 321.
(8) Ishiguro, T.; Yamaji, K.; Saito, G. *Organic Superconductors*; Springer: Berlin, 1997. Williams, J. M.; Ferraro, J. R.; Thorn, R. J. *Organic Superconductors (Including Fullerenes: Synthesis, Structure, Properties, and Theory)*; Prentice Hall: 1991. Wosnitza, J. *Fermi Surfaces of Low-Dimensional Organic Metals and Superconductors*; Springer: Berlin, 1996.
(9) Slichter, C. P. *Principles of Magnetic Resonance*; Springer: Berlin, 1989. Abragam, A. *The Principles of Nuclear Magnetism*; Clarendon: Oxford, U.K., 1961.
(10) Mori, H.; Tanaka, S.; Oshima, M.; Saito, G.; Mori, T.; Maruyama, Y.; Inokuchi, H. *Bull. Chem. Soc. Jpn*. **1990**, *63*, 2183.
(11) Mori, T. (private communication).
(12) Mayaffre, H.; Wzietek, P.; Lenoir, C.; Jerome, D.; Batail, P. *Europhys. Lett*. **1994**, *28*, 205.
(13) De Soto, S. M.; Slichter, C. P.; Kini, A. M.; Wang, H. H.; Geiser, U.; Williams, J. M. *Phys. Rev. B* **1995**, *52*, 10364.
(14) Larsen, J.; Lenoir, C. *Synthesis* **1989**, 134.
(15) Kawamoto, A.; Miyagawa, K.; Nakazawa, Y.; Kanoda, K. *Phys. Rev. Lett.* **1995**, *74*, 3455. Kawamoto, A.; Miyagawa, K.; Nakazawa, Y.; Kanoda, K. *Phys. Rev. B* **1995**, *52*, 15522.
(16) Nakamura, T.; Nobutori, T.; Miyano, M.; Tsubokura, Y.; Tsuchiya, R.; Takahashi, T.; Kanoda, K.; Saito, G. *J. Supercond*. **1994**, *7*, 671.
(17) Welp, U.; Fleshler, S.; Kwok, W. K.; Crabtree, G. W.; Carlson, K. D.; Wang, H. H.; Geiser, U.; Williams, J. M.; Hitsman, V. M. *Phys. Rev. Lett*. **1992**, *69*, 840.
(18) Kawamoto, A.; Miyagawa, K.; Kanoda, K. *Phys. Rev. B* **1997**, *55*, 14140.
(19) Kanoda, K.; Tsubokura, Y.; Ikeda, K.; Takahashi, T.; Matsukawa, T.; Saito, G.; Mori, H.; Mori, T.; Hilti, B.; Zambounis, J. S. *Synth. Met*. **1993**, *55−57*, 2865.
(20) Lefebvre, S.; Wzietek, P.; Brown, S.; Bourbonnais, C.; Jerome, D.; Mezicre, C.; Fourimigue, M.; Batail, P. *Phys. Rev. Lett*. **2000**, *85*, 5420.
(21) Kanoda, K.; Akiba, K.; Suzuki, K.; Takahashi, T.; Saito, G. *Phys. Rev. Lett*. **1990**, *65*, 1271.
(22) Carrington, A.; Bonalde, I. J.; Prozorov, R.; Giannetta, R. W.; Kini, A. M.; Schlueter, J.; Wang, H. H.; Geiser, U.; Williams, J. M. *Phys. Rev. Lett*. **1999**, *83*, 4172.
(23) Pinteric, M.; Tomic, S.; Prestrer, M.; Drobac, D.; Milat, O.; Maki, K.; Schweitzer, D.; Heinen, I.; Strunz, W. *Phys. Rev. B* **2000**, *61*, 7033.
(24) Pinteric, M.; Tomic, S.; Prester, M.; Drobac, D.; Maki, K. *Phys. Rev. B* **2002**, *66*, 174521.
(25) Harshman, D. R.; Fiary, A. T.; Haddon, R. C.; Kaplan, M. L.; Pfiz, T.; Koster, E.; Shinkoda, I.; Williams, D. L. *Phys. Rev. B* **1994**, *49*, 12990.

(26) Le, L. P.; Luke, G. M.; Sternlieb, B. J.; Wu, W. D.; Uemura, Y. J.; Brewer, J. H.; Riseman, T. M.; Stronach, C. E.; Saito, G.; Yamochi, H.; Wang, H. H.; Kini, A. M.; Carlson, K. D.; Williams, J. M. *Phys. Rev. Lett*. **1992**, *68*, 1923.
(27) Dressel, M.; Klein, O.; Gruner, G.; Carlson, K. D.; Wong, H. H.; Williams, J. M. *Phys. Rev. B* **1994**, *50*, 13603.
(28) Achkir, D.; Poirer, M.; Bourbonnas, C.; Qurion, G.; Lenoir, C.; Batail, P.; Jérome, D. *Phys. Rev. B* **1993**, *47*, 11595.
(29) Lang, M.; Toyota, N.; Sasaki, T.; Sato, H. *Phys. Rev. Lett*. **1992**, *69*, 1443.
(30) Lang, M.; Steglich, F.; Toyota, N.; Sasaki, T. *Phys. Rev. B* **1994**, *49*, 15227.
(31) Nakazawa, Y.; Kanoda, K. *Phys. Rev. B* **1997**, *55*, 8670.
(32) Elsinger, H.; Wosnitza, J.; Wanka, S.; Hagel, J.; Schweitzer, D.; Strunz, W. *Phys. Rev. Lett*. **2000**, *84*, 6098.
(33) Kovalev, A. E.; Ishiguro, T.; Yamada, J.; Takasaki, S.; Anzai, H. *J. Exp. Theor. Phys*. **2001**, *92*, 1035.
(34) Müller, J.; Lang, M.; Helfrich, R.; Steglich, F.; Sasaki, T. *Phys. Rev. B* **2002**, *65*, 140509.
(35) Arai, T.; Ichimura, K.; Nomura, K.; Takasaki, S.; Nakatsuji, S.; Anzai, H. *Phys. Rev. B* **2001**, *63*, 104518.
(36) Belin, S.; Behnia, K.; Deluzet, A. *Phys. Rev. Lett*. **1998**, *81*, 4728.
(37) Izawa, K.; Yamaguchi, H.; Sasaki, T.; Matuda, Y. *Phys. Rev. Lett*. **2002**, *88*, 27002.
(38) Schrama, J. M.; Rzephniewski, E.; Edwards, R. S.; Singleton, J.; Ardavan, A.; Kurmoo, K.; Day, P. *Phys. Rev. Lett*. **1999**, *83*, 3041.
(39) Mayaffre, H.; Wzietek, P.; Jerome, D.; Brazovskii, S. *Phys. Rev. Lett*. **1996**, *76*, 4951.
(40) Mansky, P. A.; Chaikin, P. M.; Haddon, R. C. *Phys. Rev. B* **1994**, *50*, 15929.
(41) Kanoda, K.; Miyagawa, K.; Kawamoto, A.; Nakazawa, Y. *Phys. Rev. B* **1996**, *54*, 76.
(42) Yamaji, K. *Solid State Commun.* **1987**, *61*, 413.
(43) Girlando, A.; Masino, M.; Brillante, A.; Della Valle, R. G.; Venuti, E. *Phys. Rev. B* **2002**, *66*, 100507.
(44) Schmalian, J. *Phys. Rev. Lett*. **1998**, *81*, 4232.
(45) Kino, H.; Kontani, H. *J. Phys. Soc. Jpn*. **1998**, *67*, 3691.
(46) Kondo, H.; Moriya, T. *J. Phys. Soc. Jpn*. **1998**, *67*, 3695.
(47) Vojta, M.; Dagotto, E. *Phys. Rev. B* **1999**, *59*, R713.
(48) Kuroki, K.; Aoki, H. *Phys. Rev. B* **1999**, *60*, 3060.
(49) Murakami, S.; Nagaosa, N. *J. Phys. Soc. Jpn*. **2000**, *69*, 2395.
(50) Miyagawa, K.; Kawamoto, A.; Nakazawa, Y.; Kanoda, K. *Phys. Rev. Lett.* **1995**, *75*, 1174.
(51) Takahashi, T.; Tokiwa, T.; Kanoda, K.; Urayama, H.; Yamochi, H.; Saito, G. *Synth. Met*. **1988**, *27*, 319. Skripov, A. V.; Stepanov, A. P. *Physica C* **1992**, *197*, 89.
(52) De Soto, S. M.; Slichter, C. P.; Wang, H. H.; Geiser, U.; Williams, J. *Phys. Rev. Lett*. **1993**, *70*, 2956. Kanoda, K.; Sakao, K.; Takahashi, T.; Komatsu, T.; Saito, G. *Physica C* **1991**, *185*−*189*, 2667.
(53) Mori, T. (private communication).
(54) Miyagawa, K.; Kawamoto, A.; Uchida, K.; Kanoda, K. *Physica B* **2000**, *284*−*288*, 1589.
(55) Takahashi, T.; Maniwa, Y.; Kawamura, H.; Saito, G. *J. Phys. Soc. Jpn*. **1986**, *55*, 1364. Delrie, J. M.; Roger, M.; Toffano, Z.; Moradpour, A.; Bechgaard, K. *J. Phys. (Paris)* **1986**, *47*, 839.
(56) Yamauchi, Y.; Kartsovnik, M. V.; Ishiguro, T.; Kubota, M.; Saito, G. *J. Phys. Soc. Jpn*. **1995**, *65*, 354.
(57) Smith, D. F.; De Soto, S. M.; Slichter, C. P.; Schlueter, J. A.; Kini, A. M.; Daugherty, R. G. *Phys. Rev. B* **2003**, *68*, 024512.
(58) Pinteric, M.; Miljak, M.; Biskup, N.; Milat, O.; Aviani, I.; Tomic, S.; Schweitzer, D.; Strunz, W.; Heinen, I. *Eur. Phys. J. B* **1999**, *11*, 217.
(59) Tokumoto, M.; Anzai, N.; Ishiguro, T.; Saito, G.; Kobayashi, H.; Kato, R.; Kobayashi, A. *Synth. Met*. **1987**, *19*, 215.
(60) Yoneyama, N.; Miyazaki, A.; Enoki, T.; Saito, G. *Synth. Met*. **1997**, *86*, 2029.
(61) Miyagawa, K.; Kawamoto, A.; Kanoda, K. *Phys. Rev. Lett*. **2002**, *89*, 017003.
(62) Nogami, Y.; Pouget, J. P.; Ito, H.; Ishiguro, T.; Saito, G. *Solid State Commun*. **1994**, *89*, 113.
(63) Limelette, P.; Wzietek, P.; Florens, S.; Georges, A.; Costi, T. A.; Pasquier, C.; Jerome, D.; Meziere, C.; Batail, P. *Phys. Rev. Lett.* **2003**, *91*, 016401.
(64) Kagawa, F.; Itou, T.; Miyagawa, K.; Kanoda, K. *Phys. Rev. B* **2004**, *69*, 064511.
(65) Kagawa, F.; Itou, T.; Miyagawa, K.; Kanoda, K. *Phys. Rev. Lett.* **2004**, *93*, 127001.
(66) Barthel, E.; Quirion, G.; Wzietek, P.; Jerome, D.; Christensen, J. B.; Jorgensen, M.; Bechgaard, K. *Europhys. Lett*. **1993**, *21*, 87.
(67) Tokumoto, M.; Kinoshita, N.; Tanaka, Y.; Anzai, H. *J. Phys. Soc. Jpn*. **1991**, *60*, 1426.
(68) For example: Timusk, T.; Statt, B. *Rep. Prog. Phys*. **1999**, *62*, 61.
(69) Shimizu, Y.; Miyagawa, K.; Kanoda, K.; Maesato, M.; Saito, G. *Phys. Rev. Lett*. **2003**, *91*, 107001.
(70) Komatsu, T.; Matsukawa, N.; Inoue, T.; Saito, G. *J. Phys. Soc. Jpn*. **1996**, *65*, 1340.
(71) Kurosaki, Y.; Shimizu, Y.; Miyagawa, K.; Kanoda, K.; Saito, G. preprint.
(72) McKenzie, R. H. *Science* **1997**, *278*, 820.

CR0306541